Universitat Autònoma de Barcelona

Astrocyte-targeted production of IL-10 reduces the neuroinflammatory response associated to TBI and improves neurodegeneration

Mahsa Shanaki Bavarsad

Universitat Autònoma de Barcelona

Institut de Neurociències

Dept. Cell Biology, Physiology and Immunology

Astrocyte-targeted production of IL-10 reduces the neuroinflammatory response associated to TBI and improves neurodegeneration

Mahsa Shanaki Bavarsad

PhD. Director: Dr. Beatriz Almolda Ardid

PhD. Academic Tutor: Dr. Bernardo Castellano López

Doctor of Philosophy Research Thesis

PhD in Neuroscience

Bellaterra 2020

This dissertation has been developed in the Department of Cell Biology, Physiology and Immunology and the Institute of Neurosciences affiliated with the Universitat Autònoma de Barcelona, under the direction of Dr. Beatriz Almolda Ardid.

_____	_____
Mahsa Shanaki Bavarsad	Dr. Beatriz Almolda Ardid

Bellaterra 2020

Disclaimer

I hereby declare that this dissertation is an original academic research of mine, and that it has not been submitted prior to this date to any institute for the purpose of assessment or otherwise. Furthermore, I have acknowledged all sources used, duly citing them in the reference section.

Dedication

This dissertation is dedicated to:

My parents, who have been the blaze of the sun that illuminated and warmed my path in life;

My sister, whose very presence inspired meaning in my being;

And finally, my deceased grandmother, may her soul be blessed, who taught me the practical lessons of living.

Acknowledgments

First and foremost, my thanks and appreciation are due my advisor, dear Bea, without whose support and guidance during my graduate program I could not have accomplished my PhD. My dear Bea has always encouraged me to get my work done despite the shortcomings I encountered at times. When my results, for example, were not commendable, her advice was to keep on trying, adding “results are results any way, this is science.” She never denied me her support when I shared my results and even concerns regarding my study program, listening patiently, then would give her detailed explanations to relieve me of the tensions built up thereby and pinpoint the way forward. I am truly grateful for the opportunity she gave me to learn from her and to develop the attitude of how to think scientifically, and above all, how to keep calm and remain steadfast when under duress.

My special gratitude goes to dear Berta and Bernardo for their support in many areas of concern to me, be it the dividing of animals or conducting surgery after Porto seminar. When I was dispirited for personal reasons or otherwise, they were available to attentively listen to my problems and admonish me accordingly. Their availability was heartening and a source of inspiration. I should confess that I felt at loss whenever Bernardo was not around due to his health problem during the first year of my program.

Also, I would like to thank my friends Gemma, Mireia, Ariadna, Paula, Miguel and Isabel, with whom I had very good time on different occasions. The pleasant moments daily spent chatting with dear Ariadna are unforgettable. Very special thanks are due Mireia and Paula for their considerable assistance in drafting the last part of this dissertation.

My gratefulness is also due Gemma, who, when my accommodation lease was over and I had difficult time finding a new place, kindly offered that I could stay with her. Her friendly gesture meant the world to me at the time and resonated with me the beauties of life, reminding one that the world is not depleted of great amiable people.

Special thanks go to one, who never said no to my requests, namely dear Miguel. His agreeable responses came in the form of a question: “how many slides do you have”? And at end of experiment he used to say,

“working with your slides is difficult, Mahsa, you should talk to Bea.” Having heard that, I would leave him with a smile, intuitively assured of his support and the pleasing outcome. Thank you Miguel.

I am grateful for the unforgettable wonderful time I had with the participants of the year-end gatherings, at Calçots ceremony held at Bea’s place and the summer gatherings in Bernard’s coastal house. How can I forget the pleasant time we had together theses years?

I would like also to express my thankfulness to Anna Castellano, whose very presence in the Medical College corridors was a blessing to me foreboding nice happenings for the day. (This feeling of mine I shared with her on several occasions).

I am grateful to Dr. Antonio Armario, Dr. Esther and Dr. Udina and Mercè Giralt Carbonell the Commission Members of Annual Evaluation, who were helpful in promoting the quality of my work.

I am grateful to José Rodríguez, Isabel Fernandez and Gemma Guillazo of the Neuroscience Institute who assisted me with official work, and all those whose names I don’t know, but can recognize them by their smiling faces that are associated with cordial short talks we sometimes enjoyed.

My gratitude should be shared with Mr. Nabhani, who has been of great help in solving computer problems I sometimes faced during my study.

Aside from the above, I feel obliged to express my deep appreciation to my relatives and siblings for all kinds of backing and advocacy they extended to me during my graduate program: my aunts, uncles and cousins for their incessant encouragement; especially aunt Esmat, who was undoubtedly unique in her availability to give me her apt counseling; my only sister, Mehrnoosh, who has always been my safe haven in every moment of my life; and, my brothers, Kaveh and Koosha, who were my reassurances in life.

Above all, I am indebted to my parents, who always wanted to make sure that I would develop into a mature and sophisticated person. They never stopped short of generous financial and moral support. I cannot think of meaningful life without them.

Epigraph

"If the tree of your knowledge bears fruit, you can take control of the Cosmic Wheel."

Naser Khous

Index

List of Abbreviations_____**1**

Summary_____**6**

Introduction_____**7**

Traumatic Brain Injury

Animal models of TBI

- Cryogenic model of TBI
- Fluid percussion injury models (FPI)
- Controlled cortical impact injury model (CCI)
- Weight-drop model

Acute inflammation after traumatic brain injury

Cellular components of acute inflammation

Microglial cells

Microglial cell activation and polarization

- M1 phenotype
- M2 phenotype

Astrocytes in TBI

Immune peripheral cells

Neutrophils

Monocytes

T cells

Blood Brain Barrier

Production of immune mediators

Interleukin -10 (IL-10)

Objectives_____**21**

Material and Methods_____**22**

Results_____**32**

1.Transgene-encoded IL-10 does not make any changes in the brain cyto-architecture.

2.IL-10 upregulation showed a neuroprotective role at early time-points after TBI.
3.Microglial cell activation and morphology.

4.IL-10 induces an increase in microglial cell density in basal conditions and at 3dpi.

5. Transgene-encoded IL-10 induces an inhibitory role in microglia proliferation.

6. Transgene expression of IL-10 increased the number of infiltrated monocytes.

7. IL-10 does not modify the phagocytic capacity of microglia/macrophage populations after TBI.

8. Transgene-encoded IL10 does not make any changes in microglia antigen - presenting activation.

9. Transgenic production of IL-10 modified the infiltration of peripheral immune cells.

10. Blood brain barrier permeability.

11. Transgene-encoded IL10 modifies GFAP expression in astrocytes.

12. Transgenic IL-10 production decreases the expression of IL-1β after TBI.

13. Astrocytes are the principal cells expressing the IL-10 receptor (IL-10R) in both NL and after TBI.

Discussion_____**53**

Conclusions_____ **60**

Bibliography_____ **62**

List of Abbreviations

AD	Alzheimer's Disease
AI	Area × Intensity
APC	Allophycocyanin
ANOVA	Analysis Of Variance
APC-Cy7	Allophycocyanin – Cy7
Arg1	Arginase 1
BB	Blocking Buffer
BBB	Blood Brain Barrier
B-cell	B Lymphocyte
BSA	Bovine Serum Albumin
CCI	Controlled Cortical Impact Injury
CCL2	Chemokine C-C Motif Ligand 2
CCL7	Chemokine C-C Motif Ligand 7
CCL8	Chemokine C-C Motif Ligand 8
CCL12	Chemokine C-C Motif Ligand 12
CCL13	Chemokine C-C motif Ligand 13
CCR2	C-C Chemokine Receptor Type 2
CDC	Centers for Disease Control and Prevention
CD3	Cluster of Differentiation 3
CD4	Cluster of Differentiation 4
CD11b	Cluster of Differentiation 11B
CD14	Cluster of Differentiation14
CD16	Cluster of Differentiation16
CD16/32	Cluster of Differentiation16/32
CD32	Cluster of Differentiation 32

CD45	Cluster of Differentiation 45
CD68	Cluster of Differentiation 68
CD86	Cluster of Differentiation86
CD115	Cluster of Differentiation115
CD163	Cluster of Differentiation163
CD206	Cluster of Differentiation206
CNS	Central Nervous System
CXCL9	Chemokine CXC Motif Ligand 9
CXCL10	Chemokine CXC Motif Ligand 10
CXCR2	CXC Chemokine Receptor 2
CX3CR1	CX3C Chemokine Receptor1
DAB	3,3 Diaminobenzidine
DAMPs	Damage-Associated Molecular Pattern Molecules
DAPI	4,6-Diamidino-2-Phenylindole
dH20	Distilled Water
DNA	Deoxyribonucleic Acid
DNase I	Deoxyribonuclease I
dpi	Day Post Injury
F4/80	Cell Surface Glycoprotein F4/80
FACS	Fluorescence-Activated Cell Sorting
FBS	Fetal Bovine Serum
Fc	Flowcytometry
FcR	Fc receptor
FITC	Fluorescein Isothiocyanate
Fizz1	Found in Inflammatory Zone 1
F-j B	Fluoro -Jade B
FPI	Fluid Percussion Injury
GFAP	Glial Fibrillary Acidic Protein
GFAP-IL10Tg	Glial Fibrillary Acidic Protein- Interleukin 10 Transgenic
GM-CSF	Granulocyte-Macrophage Colony-Stimulating Factor

h	Hour
H2O2	Hydrogen Peroxide
HBSS	Hank’s Balanced Salt Solution
HMGB1	High Mobility Group Box 1
hpi	Hour Post Injury
HSP	Heat Shock Proteins
Iba1	Ionized calcium binding adaptor molecule 1
ICAM-1	Intercellular Adhesion Molecule-1
IFN-γ	Interferon-Gamma
IgG	Immunoglobulin G
IHC	Immunohistochemistry
IL-1 β	Interleukin-1Beta
IL-4	Interleukin-4
IL-4Ra	Interleukin-4 Receptor Alpha
IL-6	Interleukin-6
IL-8	Interleukin-8
IL-10	Interleukin-10
IL-10R1	Interleukin-10 Receptor 1
IL-12	Interleukin-12
IL-13	Interleukin-13
iNOS	Inducible Nitric Oxide Synthase
ITCN	Image-based Tool for Counting Nuclei
LPS	Lipopolysaccharide
ly6c	Lymphocyte Antigen 6 Complex
M1	Classically Activated Macrophages
M2	Alternatively Activated Macrophages
MAPK	Mitogen-Activated Protein Kinase
MCP-1	Monocytes Chemoattractant Protein-1
MHC-ll	Major Histocompatibility Complex ll
MIP-2	Macrophage Inflammatory Protein-2

MPO	Myeloperoxidase
Mno4K	Potassium Permanganate
mRNA	Messenger Ribonucleic Acid
Mtran	Mixed Transitional
NF-κB	Nuclear Factor-Kappa B
NINDS	National Institute of Neurological Disorders and Stroke
NK	Natural Killer
NL	Non-lesioned
NL GFAP-IL10Tg 10Transgenic	Non Lesioned Glial Fibrillary Acidic Protein- Interleukin
NLWT	Non Lesioned Wild Type
OEF	Operation Enduring Freedom
OIF	Operation Iraqi Freedom
PBS	Phosphate Buffer Saline
PD	Parkinson's Disease
PE	Phycoerythrin
PE-Cy7	Phycoerythrin – Cy7
PerCP	Peridinin Chlorophyll Protein
PFA	Paraformaldehyde
pH3	Phosphohistone 3
PLP	Peri-Lesional Part
Pu.1	Transcription Factor Pu.1
RAG1	Recombination Activating Gene 1
rpm	Revolutions per Minute
RNA	Ribonucleic Acid
RNS	Reactive Nitrogen Species
ROS	Reactive Oxygen Species
RT	Room Temperature

SCI	Spinal Cord Injury
SEM	Standard Error of the Mean
SOCS3	Suppressor Of Cytokine Signalling 3
TB	Trizma Base
TBI	Traumatic Brain Injury
TBS	Trizma Base Saline
TBST 0.1%	Trizma Base Saline +1%Triton x-100
T cells	T Lymphocyte Cells
TF	Phosphate Buffer
TGF-β	Transforming Growth Factor-Beta
Th2	Type 2 T Lymphocyte helper
Th1	Type 1 T Lymphocyte helper
Th17	T Lymphocyte helper 17
TLRs	Toll Like Receptors
TNF-α	Tumour Necrosis Factor-Alpha
Tregs	T Lymphocyte Regulatory Cells
TREM2	Triggering Receptor Expressed on Myeloid cells 2
WHO	World Health Organization
WT	Wild Type
Ym1	Lectin Ym1

Summary

Inflammatory is essential in responses to peripheral infections and damage. Benefits of inflammation can be achieved if this phenomenon is controlled and for a defined period of time. Unregulated, sustained or excessive inflammation is the major cause of different neuropathologies. In the central nervous system (CNS), cerebral neuroinflammatory response after traumatic brain injury (TBI) has been characterized in patients and in different experimental animal models as one of the main causes of secondary injury leading to neuronal degeneration. Neuroinflammation is characterized by glial cell activation, leukocyte recruitment, and upregulation and secretion of cytokines and chemokines mediators. In addition, blood brain barrier (BBB) impairment has an important role in the acute time after TBI, allowing the entry of circulating neutrophils, monocytes, and T lymphocytes to the site of injury, and thus affecting neuronal death.

In different studies the crucial role of anti-inflammatory cytokines in reduction of neuroinflammatory responses have been demonstrated.

In this context, the objective of the present PhD was to characterize the effects of local production of IL-10 on the neuroinflammatory response characteristic of TBI. To achieve that cryogenic lesion model of TBI was applied to transgenic animals producing IL-10 under the astrocytic promoter GFAP (GFAP-IL10Tg animals) and their wild type counterparts, and different features of the neuroinflammatory response analyzed.

This work revealed that IL-10 promotes the survival of neurons in the early hours after injury by inhibiting glia cell activation, neutrophil recruitment, disruption of BBB and the expression levels of the proinflammatory cytokine IL-1β, associated with increased T lymphocytes infiltration. These results point to IL-10 as a good candidate to ameliorate the neuroinflammatory response after TBI and prevent secondary tissue damage.

Introduction

Traumatic Brain Injury (TBI)

External forces such as penetrating objects or a bump, blow or shake to the head that cause cognitive, psychological, neurological, and anatomical alterations in the brain, lead to traumatic brain injury (TBI). TBI has received major attention due to intense military conflicts worldwide, sport related injuries, and injuries among toddler and senior populations. According to a report by Disease Control and Prevention Center (CDC), 53,000 people die from TBI-related incidents every year in the United States (Coronado et al., 2011). This number does not include injuries seen at military or Veterans Health Administration health facilities. The National Institute of Neurological Disorders and Stroke (NINDS) reports that as many as 1.4 million people experience a TBI every year, out of which 50,000 cases die, 1 million is treated in hospital emergency rooms, and 230,000 are hospitalized and survive.

Depending on the intensity and the cause of injury the brain damage exert is to different extents and in different degrees. As a result of TBI, the brain faces massive cell loss and inflammatory events that leads to a secondary progressive neurodegeneration of neighbouring cells.

Traumatic brain injury (TBI) is complex and multifactorial damage, mainly described by primary and secondary injury. Initial injury is the result of mechanical insult and disruption of brain tissue. Molecular and biochemical changes started within minutes after the primary impact, termed secondary injury. Secondary injury processes, such as inflammation, ischaemia, blood brain barrier disruption, vasogenic edema, apoptosis and necrosis are critical in determining the extent of injury expansion and damage to brain tissue following the primary insult (Greve and Zink et al., 2009). If the incidents that follow brain injury are not controlled on time, they may spread to healthy areas beyond the main injury area and exacerbate the immune response in the central nervous system (CNS). Thus, urgent care and effective treatment should be available to TBI patients in the short and long term to treat their head injuries.

TBI is a heterogeneous disease in terms of cause, pathology, severity and prognosis. Therefore, it is hard to anticipate expected outcomes for individual patients (Ghajar et al., 20006). Significant consequences of TBI are more than half of the survivors are moderately or severely disabled one year after injury (Thornhill et al., 2000). Apart from permanent physical disabilities, TBI can be recognized as

a chronic process associated with a number of irreversible pathological conditions. Increased symptoms of seizures, sleep disorders, neurodegenerative diseases, psychiatric diseases, sexual dysfunction, bladder and bowel incontinence, and systemic metabolic dysregulation may arise and/or persist for months to years after injury (Masel and DeWitt et al., 2010). Regardless progression in understanding the pathophysiological processes of TBI during the last decades, many unanswered questions still unclear.

Indeed, no effective treatment has been approved for the TBI by any health agency in the world. Among the complex cascade of secondary events, neuroinflammation is a major pathological process in the post-TBI secondary response. Neuroinflammation by stimulating and involving multiple cell types within the CNS, is sometimes considered a double-edged sword, as can induce both detrimental and healing effects (Cederberg and Siesjo et al., 2010; Cole et al., 1986; Hagemann et al., 2007; Doyle and Buckwalter et al., 2012; Cerecedo-Lopez et al., 2014). A better understading of the neuroinflammatory response may then help in finding a good therapy for TBI.

Animal models of TBI

There are several animal models of TBI established that reflect different features of the human head injuries.

Cryogenic model of TBI

Cryogenic model has been described first by Klatzo (Klatzo et al., 1958; Albert-Weissenberger et al., 2010). The injury is delivered to the skull of animal by applying of a cold rod (for exemple using a cylinder or container filed with liquid nitrogen (-183°C) or a dry ice pieces directly applied over the skull). The cryogenic model produces focal brain injury. The primary lesion is circumscribed by a penumbral zone in which secondary pathological processes lead to neuronal death.
There are common pathological an histological characteristics between cryogenic model and human head injury such as expression of pro-inflammatory cytokines within 24 hour after injury, disruption of blood brain barrier at the early hours leading to swelling, vasogenic aedema and inflammation. This model is a useful model to study and asses the long - term neurodegenerative changes which is similar to late complications of human head injury such as impairment in cognitive and behaviour outcome. In addition, easy and simplicity in performing of lesion and highly reproducible in lesion size and location make it useful to evaluate pathophysiological processes of the secondary lesion expansion at the cortical impact site, monitor the effect of pharmacologic treatment. Lack of mechanical injury

and contra coup and diffuse axonal injury are disadvantages of this model (Raslan and Schwarz et al., 2010; Sire´n et al., 2006).

Fluid percussion injury models (FPI)

The FPI model is one of the most widely-used experimental animal model of TBI. In FPI model, the animals are subjected to craniotomy and an insult is applied by a fluid pressure pulse to the intact dura mater, producing a brief deformation of the tissue. Based on craniotomy position far away from the sagittal suture, FPI models can be classified into midline (cantered on the sagittal suture), parasagittal (<3.5 mm lateral to midline) and lateral models (>3.5 mm lateral to midline; LFPI) (Albert-Weissenberger et al., 2010; Kabadi et al., 2010). FPI models deliver reproducible injury that mimics human clinical TBI without skull fracture and reflect aspects of contusion, diffuse axonal injury, intracranial haemorrhage, brain swelling and progressive grey matter damage. Both focal and diffuse injury can be produced by this model. The degree of damage depends on two parameters, craniotomy location and injury severity (the strength of the pressure pulse).

Controlled cortical impact injury model (CCI)

A piston or rigid impactor is driven by air pressure or electromagnetism onto the exposed dura through craniotomy at a controlled angle, velocity and depth. (Albert-Weissenberger et al., 2010) CCI model induces cortical brain contusion, haemorrhage, blood brain barrier, vasogenic edema disruption, neuronal cell death and degeneration, astrogliosis, microglial activation, inflammatory events, axonal damage and cognitive deficits. CCI model generates both focal cortical and diffuse sub cortical injuries.
The predominantly focal brain injury caused by CCI makes this model to a useful tool for studying the pathophysiology of the secondary processes induced by focal brain injury (Dixon et al., 1991; Lighthall et al., 1990).

Weight-drop model

In weight- drop model injury (Feeney's weight-drop and Shohami's weight-drop) is delivered to the exposed skull (with or without a craniotomy) in ~~the marine~~ animals by use of the gravitational forces of a free falling weight and producing both focal and diffuse injuries. (Albert-Weissenberger et al., 2010; Morales et al., 2005). Adjusting the mass of the weight and the height from which it falls can alter injury severity in these models.
Weight-drop model induces cortical brain contusion, haemorrhage, BBB breakdown, neurological impairment, astrogliosis, microglial activation,

inflammatory events and axonal damage. No long-term studies have evaluated behavioural dysfunction after weight drop TBI and it remains a poorly understood. The weight drop model represents a quick, easy, and convenient technique. One disadvantage of this model involves the increased probability of skull fractures at higher magnitudes of injury severity (Albert-Weissenberger, Varrallyay and Raslan et al., 2012; Feeney and Boyeson et al., 1981).

Acute inflammation after traumatic brain injury

A dramatic and robust inflammatory response develops acutely after injury and is characterized by 1) the activation of CNS resident cells (microglia and astrocytes), 2) the migration and recruitment of peripheral leukocytes, and 3) the release of inflammatory mediators (Soares et al., 1995; Ziebell et el., 2010). Within minutes and hours after the injury, cellular damage associated with the mechanical impact release certain number of endogenous components, such as RNA, DNA, heat shock proteins (HSP), and HMGB1 (high mobility group box 1), which act as damage associated molecular patterns (DAMPs) (Manson et al, 2102) and signal to other cells via pattern recognition receptors, like Toll-like receptors (TLRs). CNS resident cells, including microglia, astrocytes and cerebrovascular endothelium, express molecules of the TLR family (Gurley and Nichols et al., 2008; Kigerl et al., 2014; Nagyoszi and Wilhelm et al., 2010). Binding of DAMPs to TLRs activates the nuclear factor-κB (NFκB) and MAPK signalling pathways leading to the release of a variety of pro-inflammatory factors, including cytokines (IL-1β, TNF-α IL-6), chemokines, and upregulation of immune receptors. This initial wave of inflammatory mediators serves to activate microglia and astrocytes, possibly increasing their migration, and recruit peripheral immune cells to the site of injury (Dalgard and cole et al., 2012; Soares et al., 1995; Rhodes et al., 2011). After recruitment to the brain, leukocytes initiate the production of a second wave of inflammatory mediators that contributes to the tissue damage (Soares et al., 1995). Neutrophils are the first peripheral immune cell type responding to injury. They star accumulating in the subarachnoid space and vasculature near the injury and subsequently enter into the brain parenchyma around 1 day post injury. (Soares et al., 1995; Rhodes et al., 2011). In contrast, mononuclear leukocyte accumulation predominates in the lesion later on, by 3–6 days post injury (Soares et al., 1995; Rhodes et al., 2011). Identification by immunohistochemistry and flow cytometry indicates that most recruited cells are inflammatory $CD45^{hi}CCR2^{+}$ $Ly6C^{+}$ monocytes (Hsieh et al., 2013). Leucocyte recruitment is essential for clearing tissue damage or infection, whereas recruited neutrophils and macrophages in the site of injury release reactive oxygen and nitrogen species that exacerbate tissue damage. (Liu Yang-Wuyue et al., 2108). Moreover, microglia and macrophages express MHC-II antigen presenting immunoregulatory characteristics. They mediate activation and

migration of T lymphocytes and natural killer (NK) cells to the site of injury to better resolve tissue damage. T lymphocytes and natural killer (NK) infiltrate in low numbers, but with a similar temporal profile, to monocytes (Holmin et al., 1995). At the same time, brain-resident microglia and astrocytes become activated. Microglia assume an amoeboid morphology, secrete inflammatory factors, perform phagocytosis, and are largely indistinguishable from infiltrating monocyte-derived macrophages (Soares et al., 1995; Kelley et al., 2007).
Resolution, the final phase of acute inflammatory response, takes place around 10–14 days after injury, when peripheral immune cells are largely absent. However, in some studies the presence of F4/80^{+}macrophages and glial fibrillary acidic protein (GFAP)$^{+}$ astrocytes at sites far away from the primary injury, remain in deeper brain regions such as thalamic projection, for months and even years after the primary insult, indicative of diffuse injury (Kelley et al., 2007).

It has been long established that neuroinflammation is a major contributor to secondary injury. In fact, it has been postulated that in many cases, TBI-induced neuroinflammation is more detrimental to pathological progression than the primary injury itself. Thus a major knowledge of this inflammatory response could help in the finding better therapeutic strategies to avoid the spreading of the secondary injury.

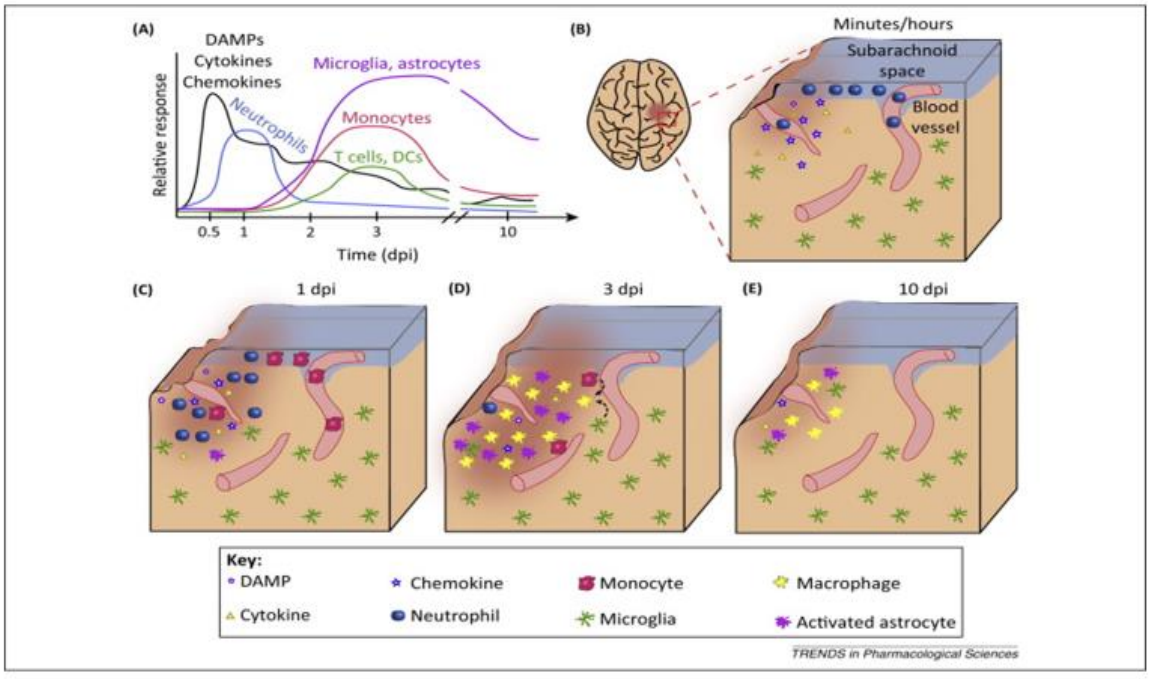

Figure 1. Inflammatory response to traumatic brain injury (TBI).

(A) Time course of molecular and cellular mediators after TBI. (B–E) Histological representation of the inflammatory reaction. Extracted from (Gyoneva and Ransohoff et al., 2015).

Cellular components of acute inflammation

As already commented the principal cellular components of the neuroinflammatory response associated to TBI are the glial response, including both microglia/macrophages and astrocytes as well as the peripheral immune cells recruited to the injured brain, principally neutrophils, monocytes and T-cells.

Microglial cells

Microglial cell activation and polarization

When the homeostasis of the CNS becomes altered as a result of acute or chronic injuries, microglial cells become activated. This microglial activation, among others, includes changes in the phenotype of the cells that depends of the nature of the injury, the severity, and the specific microenvironment in which the microglia response takes place. In an attempt to organize the wide amount of molecules and factors that microglia can produce after activation, many studies along the last years have tried to define different populations of microglia. This is how the concept of microglia polarization emerges. Microglial polarization is a relatively new concept, not without conflict, which has been already described in many studies (Ransohoff et al., 2016). This polarization concept on microglia come from the concept that, as their counterparts in peripheral tissues, the macrophages, show considerable plasticity that able them to respond to environmental signals and change their phenotype and function following pathogen exposure or tissue damage (Gordon et al., 2003; Sica and Mantovani et al., 2012). Two main distinct macrophage phenotypes have been described, the M1 and the M2-macrophage activation state (Gordon et al., 2003; Sica and Mantovani et al., 2012). Moreover, the M2 phenotype is grouped into three polarization subtypes, M2a, M2b and M2c, each with a specific function and pattern of phenotypic marker expression (Gordon et al., 2003; Sica and Mantovani et al., 2012).

M1 phenotype

The *classical* M1-like phenotype is associated with the response of macrophages to pro-inflammatory molecules, such as bacterial lipopolysaccharide (LPS) or the TH1 cytokine, interferon-γ (IFNγ). Once activated M1-cells secrete high levels of pro-inflammatory cytokines (IL-1β, IL-12, tumor necrosis factor-α (TNFα)), chemokines (CCL2, CXCL9, CXCL10), and reactive oxygen species (ROS) that are essential for host defence (Colton et al., 2009; Gordon et al., 2003; Sica and Mantovani et al., 2012). M1-like activation is associated with phagocytosis, and ROS release (Colton et al., 2009; Gordon et al., 2003; Sica and Mantovani et al., 2012)

and is characterized by specific markers such as CD16, CD32, CD86, MHC II and iNOS. In many cases, the M1-like response is protective and is downregulated after damage and pathogen removal; however, a dysregulated or excessive M1-like activation in the brain can induce neurotoxicity by releasing of pro-inflammatory factors and neurotoxic mediators that induces neurodegeneration.

M2 phenotype

In response to TH2 cytokines, such as IL-4 and IL-13, macrophages adopt an *alternative* M2a-like state that is associated with immunity against parasites, Th2 cell recruitment, tissue repair, and growth stimulation (Colton et al., 2009; Gordon et al., 2003; Sica and Mantovani et al., 2012). M2a-cells are associated with production of anti-inflammatory cytokines (IL-10), upregulation of several phenotypic markers such as arginase 1, CD206, Ym1, Fizz1, inhibition of NFkB isoforms, and high expression of phagocytotic scavenger receptors (Colton et al., 2009; Gordon et al., 2003; Sica and Mantovani et al., 2012).

In response to IL-10, glucocorticoid and TGF-β, macrophages acquire a 'deactivated' M2c-like phenotype. This phenotype appears to be involved in tissue remodelling and matrix deposition after inflammation (Colton et al., 2009; Gordon et al., 2003; Sica and Mantovani et al., 2012). Phenotypic markers of M2c- cells include CD163, CD206 and TGF-β.

Finally, in response to immune complex exposure and toll like receptors (TLRs) ligands macrophages can adopt an intermediate M2b-like phenotype (Colton et al., 2009; Gordon el al., 2003; Sica and Mantovani et al., 2012). M2b can induce either pro- or anti-inflammatory function and is associated with memory immune responses (B-cell class switching and recruitment of Treg cells). The M2b phenotype has characteristics of both M1 (MHCII, CD86) and M2 (IL-10^{high}, IL-12^{low}) phenotype. When M2b macrophages stimulate T cells they are inclined towards a Th2 response (Filardy et al., 2010), which suggests that they may be a potential regulator of the M2 response in general.

Along the last years it seems clear that this classification sometimes is very simplistic and not valid. In fact, microglia and macrophage often show mixed phenotypes indicative of their plasticity nature and their ability to acquire multiple activation phenotypes in response to local environmental signals and dynamic changes in the inflammatory milieu (Sica and Mantovani et al., 2012).

Recent data in TBI revealed that there was a transient increase in expression of M2-like microglia, mostly with TGF-β expression, in the acute phase after injury that was replaced with the persistent and predominant M1-like microglial phenotype, with iNOS and IL-12, at delayed time point (Kumar et el., 2016). Similar activation

of microglia and macrophages in spinal cord injury (SCI) and other TBI models were also reported (Kigerl and Gensel et al., 2009; Wang et al., 2013).

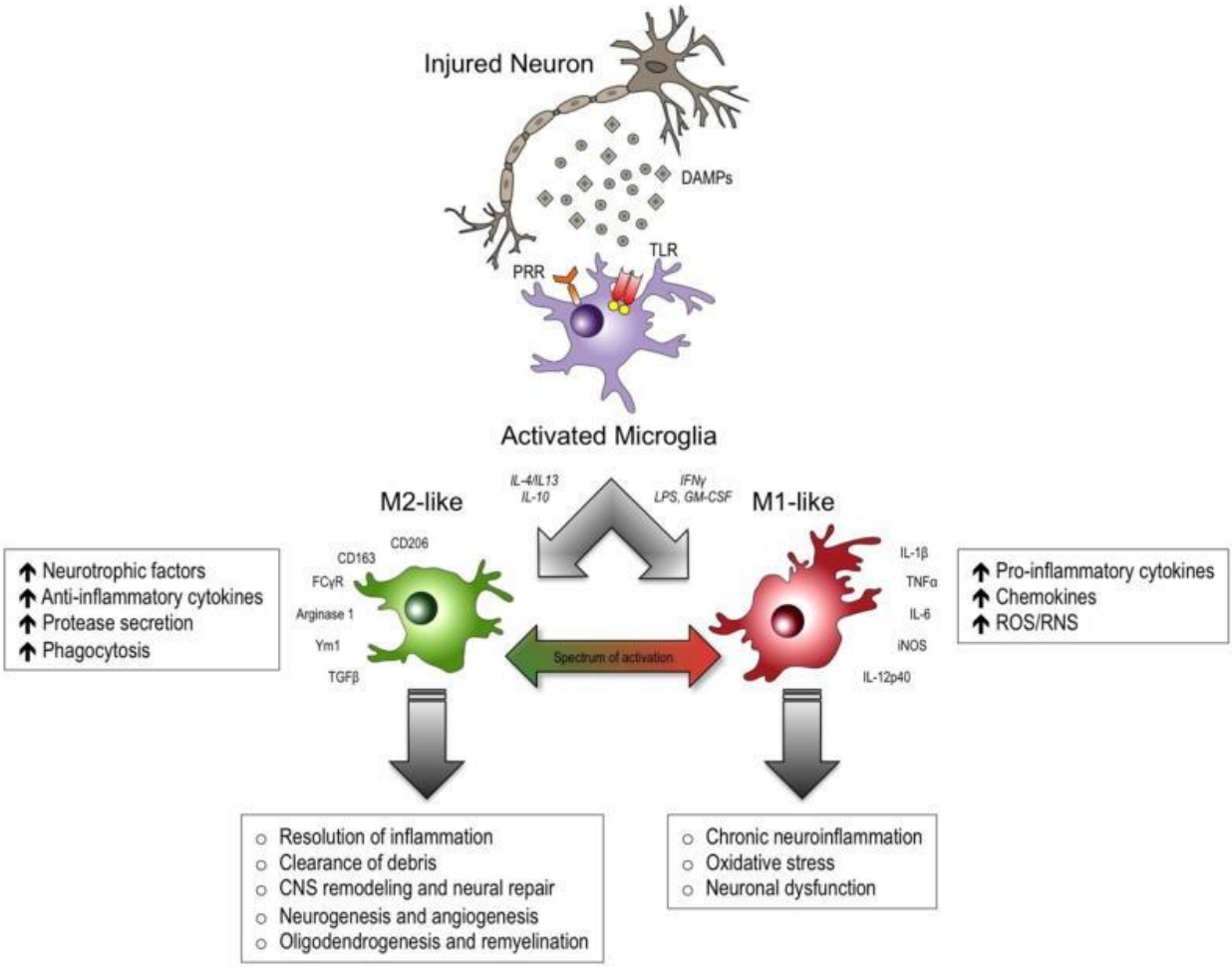

Figure 2. Microglial polarization after TBI.

M1-like and M2-like activation states that can have distinct roles in neurodegeneration and tissue repair. M1-like microglia are characterized by upregulated expression of phenotypic protein markers such as IL-1β, TNFα, IL-6, iNOS, and IL-12p40. They release pro-inflammatory cytokines, chemokines and free radicals that impair brain repair and contribute to chronic neuroinflammation, oxidative stress and long term neurological impairments. In contrast, M2-like microglia upregulate protein markers such as CD206, CD163, FCγR, arginase 1, Ym1, and TGFβ. M2-like microglia release antiinflammatory cytokines, neurotrophic factors and proteases, and they have increased phagocytic activity. M2-like microglia promote immunosuppression and resolution of M1- mediated neuroinflammation, and participate in CNS remodeling and repair by modulating neurorestorative processes such as neurogenesis, angiogenesis, oligodendrogenesis and remyelineation. Extracted from Loane and Kumar et al., 2016.

Astrocytes in TBI

In addition to microglia, astrocytes also respond to injury by morphological changes (extension of processes and swelling of cell bodies), by upregulation of intermediate filament proteins such GFAP (glial fibrillary acidic protein), by increased proliferation and by production-releasing of inflammatory cytokines and growth factors (Zamanian et al., 2012; Paintlia et al., 2013). In the mouse CCI model of TBI, reactive astrocytes are detected in the lesional and peri-lesional area at 3dpi showing the highest morphological changes associated with scar formation at 7dpi (Villapol et al., 2014). Reactive astrocytes are observed up to 60 days after in injury in this model indicating continued response of astrocyte after TBI. The role of reactive astrocytes in this injury model has be defined as both neurodegeneration and neuroprotective context. In a mouse model of moderate CCI, deletion of proliferating reactive astrocytes lead to neuronal degeneration and increased inflammation, suggesting the critical role of astrocytes in maintain neuronal survival after moderate TBI (Myer et al., 2006). However, after rat fluidic percussion injury (FPI), the suppression of proliferating astrocytes resulted in reduced neuronal degeneration associating with low scar formation, microglia activation and eventually improvement in cognitive outcome (Di Giovanni S and Movsesyan et al., 2005).

As already commented, one of the principal functions of astrocytes in TBI is the formation of the glial scar. This glial scar is comprised of, largely astrocytes, but also microglia, endothelial cells, fibroblast and extracellular matrix (Silver and Miller et al., 2004). The function of the scar is to enclosed the injured area for further damage by preventing leakage of toxic molecules into healthy tissue and also to prevent migration of cells into and out of the injured area (Ribotta, Menet and Privat et al., 2004). In addition to this protective role, the scar also show inhibitory effects on the regrowth and axonal regeneration Ribotta, Menet and Privat et al., 2004), indicating that this scar formation after injury can have both beneficial and detrimental effects.

Immune peripheral cells

Neutrophils

Neutrophils are the principal peripheral immune cells initially recruited into the site of injury after TBI. Neutrophils are apparent in subarachnoid space and large blood vessels within hours after injury, then they migrate from damaged vasculature into parenchyma, becoming predominant cell type by 24hpi (Gyoneva and Ransohoff et al., 2015; Jin and Ishii et al., 2012). Neutrophils have numerous toxic substances namely lysosomal enzymes such as myeloperoxidase, reactive oxygen species (ROS) and reactive nitrogen species (NOS), cytokines and chemokines (Liu Yang-

Wuyue et al., 2108). Neutrophils augment pathological tissue damage by producing and releasing pro-inflammatory cytokines and chemokines such as TNF-α, IL-1β and IL-8, which amplify the recruitment and activation of more neutrophils to the site of injury through upregulated endothelial adhesion molecules (Liu Yang-Wuyue et al., 2108). Production of free radicals of recruited neutrophils resulting from brain trauma alters the structure and function of cell membranes leading to increased vasogenic permeability and eventually increased in cerebral edema formation (Kenne and Erlandsson et al., 2012). However, some studies indicated that inhibition of neutrophil recruitment, by blocking adhesion molecules such as anti-CD11b and anti-ICAM-1 antibodies, reduced the neutrophil recruitment after TBI but has no effect on lesion size and neuronal deficit (Knoblach and Faden et al., 2002; Carlos and Clark et al., 1997; Weaver and Branch et al., 2000). In contrast, experiments using the CXCR2 KO mice, showed a reduction in neutrophil infiltration, associated with reduction in lesion volume and cell death after TBI, suggesting a beneficial effect of inhibition of neutrophil recruitment (Semple et al., 2010).

Monocytes

Monocytes are peripheral immune cells that generate and develop in the bone marrow constantly, circulate in the blood flow and migrate into damaged or infectious tissue where they are differentiated into tissue macrophages or dendritic cells. Monocytes are a heterogeneous population, with two major subsets in the peripheral blood, based on the differential expression level of Ly6C marker and chemokine receptor CCR2. “Inflammatory” monocytes expressing $Ly6C^{high}$ $CCR2^{high}$ $CX3CR1^{low}$ and “patrolling or circulating” monocyte identified as $Ly6C^{low}CCR2^{low}CX3CR1^{high}$ (Mildner and Marinkovic et al., 2106).

Chemokine receptor-CCR2 mainly expressed in the subset of inflammatory monocytes ($CD45^{high}$ $Ly6C^{high}$) is responsible for mobilization of monocytes out of bone marrow and migration into peripheral tissues, including the brain under pathological situations. (Gyoneva and Ransohoff et al., 2015). Chemokine receptor-CCR2 link to CCL2 (known as monocyte chemoattractant protein-1 MCP-1), CCL7, CCL8, CCL12 in mice and CCL13 in humans. (Gyoneva and Ransohoff et al., 2015). There is strong evidence about CCL2/CCR2 signalling pathway mediating acute inflammation cascade and exagerate secondary tissue damage after traumatic brain injury (TBI). In fact, $Ly6C^{high}$ inflammatory monocytes preferentially are recruited to the site of injury mainly based on the CCL2/CCR2 signalling-dependent fashion (Semple, Bye and Rancan et al., 2009; Chu et al., 2014).

After brain injury, $Ly6C^{high}$ inflammatory monocytes follow chemokine gradient, being recruited to the damaged brain, and differentiate into macrophages. Monocytes become the predominate cell type in the tissue damage at 3-5 days after injury (Soares et al*.,* 1995*;* Gyoneva and Ransohoff et al., 2015). Monocyte-derived

macrophages and activated resident microglia posses similar phenotypically and functionally characteristics. Activated microglia acquire an amoeboid morphology resembling the round phagocytic shape of monocyte-derived macrophages, making difficult to distinguish correctly between activated microglia and macrophages. However, accumulating data have revealed that these two cell types are distinct and showing some differences. For instance, microglia and macrophages have different origins, microglia are originated from the primitive ectoderm of the yolk sac, while hematopoietic stem cells are the origin for macrophages (Ginhoux and Greter et el., 2010). In addition, gene expressing profile studies demonstrate difference between these two cell types (Butovsky and Jedrychowski et al., 2104), suggesting that it may have different functions and roles after injury (Yamasaki and Butovsky et al., 2104). So that, in mice model of TBI, microglia cells are observed as first innate immune cells at the site of injury associating with phagocytosis in acute phase of injury, whereas macrophages appeared at later. Regardless of these differences, to date it is difficult to differentiate functions and roles of microglia and macrophage.

T cells

T cells constitute cellular mediators of the adaptive immunity, originated from hematopoietic stem cells and developed into the thymus (Reiner et al., 2009). T cells are classified into various subsets, cytotoxic, helper, or regulatory lymphocytes, based on their effector functions and molecular phenotype (Zhu and Yamane et al., 2010; Zhang and Bevan et al., 2011). Animal and human studies provide evidence that T cells migrated into the injured brain after TBI, during both acute and chronic phases (Jin and Ishii et al., 2012; Holmin and Soderlund et al., 1998; Dressler et al., 2007). After controlled cortical impact (CCI) T cells increase in the brain parenchyma at 3-5 days after injury reducing after that at 7 days of TBI (Jin and Ishii et al., 2012). In general the number of T cells into the brain after trauma is fewer than neutrophils and macrophages. However, to date, there are few studies about the exact role of T cells after TBI. Some studies demonstrate that T cells exacerbated the posttraumatic tissue damage (Clausen and Lorant et al., 2017). Moreover, transferring of effector CD4+ T cells adoptively into T and B cell-deficient (recombination-activating gene 1(RAG1) knockout mice) exacerbated lesion size and apoptosis after brain injury (Fee and Crumbaugh et al., 2003). In contrast, depletion of Tregs in a CCI model of TBI, lead to higher infiltration of T cells to the injured brain parenchyma associated with enhanced IFN- δ expression and exaggerated reactive astrogliosis (Krämer and Hack et al., 2019). Further research and investigation, specially determining the subtype of T-cells present in the brain parenchyma, is needed to clarify the exact role of T cells in the acute and chronic phases after TBI.

Blood Brain Barrier

The breakdown in blood-brain barrier (BBB) integrity is observed in different disorders such as ischemia (Yang C et al., 2018), Alzheimer (Zlokovic et al., 2011), multiple sclerosis (Kirk and Plumb et al., 2003) and TBI (Habgood et al., 2007; Povlishock et al., 1978).
After experimental brain trauma, vascular permeability is increased leading to brain edema and a complex sequence of inflammatory cascades (Povlishocket et al., 1978; Dietrich et al., 1994; Habgood et al., 2007). Alterations in BBB permeability may contribute to secondary brain injury by the abnormal passage of blood substances into the brain parenchyma that influence neuronal vulnerability (Stahel and Shohami et al., 2000; Lucas et al., 2006). BBB disruption has been demonstrated in the acute phase in several animal models of TBI, but the temporal course of this disruption is unclear. Some studies suggest a short term permeability of the BBB following injury which is resolved within hours (Habgood et al., 2007; Povlishock et al., 1978). Studies in TBI suggest a more dynamic biphasic course of BBB disruption, with an acute phase around 3–6 hours post injury and a later phase at 4 days post injury (Habgood et al., 2007).
In addition to the reports in animal models of TBI, evidence of acute BBB disruption has been described in TBI patients by increased serum albumin in cerebral spinal fluid (Stahel et al., 2001; Saw et al., 2014). Findings related to BBB breakdown after TBI suggests that vascular damage induced by trauma leads to migration of circulating leukocytes into the brain parenchyma (Soares et al., 1995; Schoettle et al., 1990) which may affect the microglial activation, an important component of the inflammatory response to injury and a source of a variety of chemokines and cytokines (Lu et al., 2001; Block et al., 2007).

Production of immune mediators

Cytokines are members of a large group of endogenous proteins and polypeptides. They are able to mediate a wide range of biological activities such as proliferation, differentiation and immune and inflammatory process. Cytokines normally are produced in the low or undetectable levels in the health tissue but rapidly upregulated after pathological conditions, such as TBI. Inflammation is activated after brain trauma and mediated by cytokines production secreted from activated microglia and recruited peripheral immune cells. Cytokines are considered as a potential key for secondary tissue damage (Dalgard et el., 2012; Mukherjee et al., 2011).

Several pro-inflammatory and anti-inflammatory cytokines have been reported after TBI (Dalgard et el., 2012; Mukherjee et al., 2011). Pro-inflammatory cytokines, in particular IL-1β and TNF- α have a key role in initiating and regulation of cytokines

cascade during inflammatory response. Tumour necrosis factor-α (TNF-α) expression appeared in high level very early, within the first 4 hours, in the cortical injured tissue and remain elevated for 24h after injury (Dalgard et el., 2012; Harting and Jimenez et al., 2008). Similar temporal expression profile is observed for interleukin -1β (IL-1β) (Dalgard et el., 2012). TNF-α and IL-1β have been defined as potential contributors for secondary tissue damage. They are predominantly produced by activated microglia and astrocytes in response to trauma (Shohami E. et al.,1997). Interestingly, these two proinflammatory cytokines act synergistically to induce enhanced neurotoxic effect, suggesting the crucial role of these two cytokines in mediating of neuroinflammation and secondary tissue damage (Allan and Rothwell et al., 2001; Chao et al., 1995).

Chemokines are a large subgroup of cytokines family, defined as chemotactic cytokines. They regulate the leukocyte activation and migration to the site of injury. Chemokines and their receptors are also expressed in the CNS by glial cells and neurons. Chemokines can be divided into four groups based on the presence of positionally conserved cysteine residues in their primary structure: XC, CC, CXC, and CX3C chemokines. Several chemokines and their receptors have been examined in the context of TBI. Particularly, Interleukin-8 (IL-8) or macrophage inflammatory protein-2 (MIP-2) in rodents, is a potent chemotactic factor for neutrophils which contribute to secondary brain injury (Dalgard et el., 2012; Mukherjee et al., 2011).

Monocytes chemoattractant protein (MCP-1), know also as CCL2, is one of the initial chemokine that significantly upregulated early after lesion (Dalgard et el., 2012). CCL2/CCR2 signalling pathway drive acute inflammation response after TBI, indicating a role for CCL2 in development of neuropathology after injury (Semple, Bye and Rancan et al., 2009). In the CNS the main source of CCL2 production after injury are glial cells (Rankine et al., 2006).

Interleukin -10 (IL-10)

Interleukin-10 (IL-10) is one of the main crucial immunoregulatory cytokine in the periphery where it has been linked with an anti-inflammatory function (Couper et al., 2008; Moore et al., 2001). In the CNS, IL-10 expression has been described upregulated after a wide variety of neuroinflammatory situations including traumatic brain injury (Kamm et al., 2006), middle cerebral artery occlusion (MCAO) (Zhai et al., 1997), excitotoxicity (Gonzalez et al., 2009), Alzheimer's disease (Apelt and Schliebs, 2001), multiple sclerosis (Hulshof et al., 2002) and its experimental animal model, experimental autoimmune encephalomyelitis (EAE) (Ledeboer et al., 2003). Moreover, IL-10 has been detected in the cerebrospinal fluid of patients with severe brain injury (Csuka and Morganti-Kossman et al., 1999) and in experimental brain injured rats (Kamm et al 2006). Microglia and astrocytes are the main sources of IL-10 production in the CNS.

Expression of IL-10 receptor (IL-10R) has been shown in neurons and glial cells including microglia, astrocytes and oligodendrocytes in both basal conditions and after injury (Ledeboer et al., 2002; Norden et al., 2014; Gonzalez et al., 2009; Cannella and Raine et al., 2004). Administration of IL-10 has been found to suppress microglial and astroglial activation, as well as decrease in production of proinflammatory cytokines (Lodge et al., 1996; Balasingam et al., 1996; Bethea et al., 1999) and leukocyte infiltration (Ooboshi et al., 2005). Furthermore, IL-10 showed a neuroprotective function after traumatic brain injury, excitotoxicity and MCAO among others (Arimoto et al., 2007; Bachis et al., 2001; Brewer et al., 1999; Knoblach and Faden, 1998; Ledeboer et al., 2000; Molina-Holgado et al., 2001; Ooboshi et al., 2005; Park et al., 2007; Spera et al., 1998; Xin et al., 2011). Notably, the route of administration of IL-10 seems essential for protection. Thus, after acute injuries such as spinal cord excitotoxicity or traumatic brain injury, intraspinal or intracerebroventricular IL-10 administration worsens disease (Brewer et al., 1999) or has no effect (Knoblach and Faden, 1998), whereas systemic administration improves the functional outcome of lesions (Brewer et al., 1999; Knoblach and Faden, 1998).

Objectives

Neuroinflammation is one of the crucial processes associated with the secondary injury and thus with the neurodegeneration after traumatic brain injury. This process includes glial cell activation, proinflammatory cytokines secretion, leukocyte recruitment and blood-brain barrier damage. Interleukin-10, a cytokine with anti-inflammatory and immunosuppressive properties negatively modulates inflammatory cascades at multiple levels. Based on this evidence, we hypothesize that IL-10 attenuates neuroinflammatory process after TBI reducing the secondary injury and inducing an improvement in the neuronal outcome.

The specific purposes of the current study were:

1-To determine the putative influence of astrocyte-targeted IL-10 production on neuronal degeneration associated to TBI.

2-To elucidate the influence of astrocyte-targeted IL-10 production on glial responses associated to TBI.

3-To characterize the effect of astrocyte-targeted IL-10 production on infiltration of peripheral immune cells such as neutrophils, monocytes and T cells.

4-To asses the impact of astrocyte-targeted IL-10 production on BBB permeability.

5-To analyse the possible changes that astrocyte-targeted IL-10 production induces on the cytokine-chemokine profile associated to TBI.

Methodology

Animals

Adult transgenic (GFAP-IL10Tg) mice and their corresponding Wild type (WT) littermate between four - five months old of both sexes were used in this work. GFAP-IL10Tg mice have been designed, created and characterized by our group (Almolda et al., 2015). All animals were maintained and housed in their home cages at an appropriate temperature (24±2) with 12 hour light-dark cycle and *ad libitum* access to water and food.

All experimental animal work was conducted according to Spanish regulations (Ley 32/2007, Real Decreto 1201/2005, Ley 9/2003 and Real Decreto 178/2004) in agreement with European Union directives (86/609/CEE, 91/628/CEE and 92/65/CEE) and was approved by the Ethical Committee of the Autonomous University of Barcelona.

Cryogenic brain injury

Wild type (WT) and transgenic (GFAP-IL10Tg) mice were anesthetized with an intraperitoneal injection of Ketamine (80 mg/Kg) and Xylazine (20mg/Kg) at dose of 1ml/gr per animal. Head of animals was shaved and skin cut to exposed the skull. The cryogenic lesion was performed on the right parietal skull, 2.5mm posterior and 2.5mm lateral from Bregma (Figure 3). A metal device having caoutchouc holder with a tip diameter of 2 mm were kept in liquid nitrogen (-196°C) and placed on the target point for 60 seconds contact time. Wounds were closed by standard skin suture (Laboratory Arago.S.L-6/0) and disinfected by iodine solution. Lesioned animals were placed in the warmer pad for recovery and returned to their home cage until sacrifice at 24 hours post-injury (hpi), 3 and 7 days post-lesion (dpi). Non lesioned (NL) animal of each group received the same anesthesia and surgical operation procedure but without trauma.

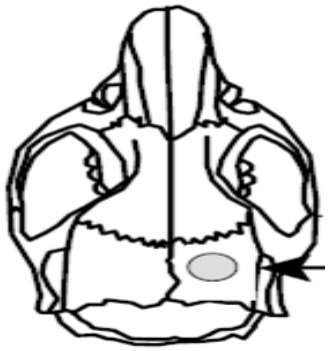

Figure 3. Focal brain lesion coordinates from bregma: 2.5 mm posterior and 2.5 mm lateral in which the cryogenic brain injury was performed (arrow).

Experimental groups

Non lesioned (NL) and lesioned animals were distributed in different experimental groups and analyzed at 24 hours, 3 and 7 days post-lesion (hpi, dpi) for immunohistochemistry (IHC), flow cytometry and protein analysis. A total of 89 WT and 93 GFAP-IL10Tg animals were used for IHC, 20 WT and 20 GFAP-IL10Tg for flow cytometry and 19 WT and 19 GFAP-IL10Tg for protein analysis.

Tissue processing for histological analysis

At the corresponding time-points, TBI-lesioned animals were anesthetized deeply with the same Ketamine (80 mg/Kg) and Xylazine (20mg/Kg) solution describe above, but at 1.5 ml/gr per animal dose and intracardially perfused with 4% paraformaldehyde buffer (4%PFA in Tris-buffer saline 0.1M pH 7.4 (TBS)) for 10 minutes. Intact brain of each animal was quickly removed and post-fixed in the same fixative solution for 4 hour at 4 ℃. Then brains were washed with cold phosphate buffer (TF 0.1M) and cryo-protected with 30 % sucrose solution in 0.1M phosphate buffer for 48h at 4℃. Brains were frozen in cold 2- methyl butane (-55 to -60 ℃) (320404, Sigma-Aldrich, St. Louis) and stored at -20 °C. Stored frozen samples were cut into 30µm parallel coronal sections by cryostat (CM 3050S Lecia) (Figure 4) mounted on the SUPERFROST® PLUS slides, dried in the oven at 37℃ for 6 hours and stored at -20℃ until used.

Figure 4. Cryostat device.

Toluidine blue Staining

One series of NL and lesioned (24hpi, 3dpi, 7dpi) WT and GFAP-TgIL10 animals were dried for 6h at RT and incubated in toluidine blue solution (0.1% toluidine blue diluted in acetate Walpole buffer (0.05M, pH 4.5)) for 1 minute at RT. After that, slides were washed with distilled water and dehydrated by graded alcohol (50%, 70%, 90, 100% ethanol), treated with xylene and cover slipped with histology mounting media.

Fluoro-Jade B staining

Sections of TBI-lesioned WT and GFAP-IL10Tg animals at all time points (24hpi, 3dpi, 7dpi) were dried for 6h at RT, dehydrated by ethanol 100% (2x1ˈ), rehydrated sections by dipping in graded ethanol 70%, 50% and finally in distilled water. After incubating in potassium permanganate oxidant solution for 15 minutes at RT (0.06 gr Mno4K solved in 100ml d.H20), sections were rinsed in dH_20 and incubated in 0.01% Fluoro-Jade B (FJ-B) solution for 20 min at RT. For making FJ-B stock solution, 96 ml dH_20, 1 ml glacial acetic acid and 4ml Fluoro-jade solution were mixed. Finally stained sections were washed with dH_20, dried and dipped in xylene and cover slipped with histology mounting.

Degenerating Neurons quantification

In order to study the number of degenerating neurons after TBI in WT and GFAP-IL10Tg animals, sections labelled with FJ-B were analysed for all time points. A minimum of nine WT and nine GFAP-IL10Tg animals were used. A total of 20 photographs from a minimum of five sections per animal including the degeneration neurons located in the penumbra were captured by using the 10x objective with a DXM 1200F Nikon digital camera joined to a brightfield Nikon Eclipse 80i microscope, using the ACT-1 2.20 (Nikon corporation) software. By means of analySIS®, the total number of degenerating FJ-B+ neurons were quantified. Data were expressed as FJ-B+ cells per section.

Lesion size quantification

In order to evaluate the size of lesion, we used the sections stained with FJ-B. A minimum of eight WT and eight GFAP-IL10Tg animals at 24hpi, 3 and 7dpi after TBI were analyzed. A minimum of five sections per animal, containing the degeneration neurons, were analyzed. Photos of each section were captured using the 2x magnification with a DXM 1200F Nikon digital camera joined to a brightfield Nikon Eclipse 80i microscope, using the ACT-1 2.20 (Nikon corporation) software. Before quantification all photos of the same section were merged together in a unique photo by Photoshop® CC software. For each final photo, the volumen of the total ipsilateral hemisphere and the lateral ventricle of the affected area were measured by using analysis® software. To determine the correct affected area, and delete the brain swelling or edema, the volume of the lateral ventricle was deducted from the ipsilateral hemisphere for each section. Volume of affected area for each section was then calculated by multiplying section thickness by the number of series and the corrected quantified affected area. Total affected volume of each animal were obtained by averaging all sections volume of the affected area. Coronal section corresponding to -0.38mm distance from Bregma (area were the center of the lesion is located) was considered as a zero point and injured frontal and caudal sections were compared with this Bregma point.

Immunohistochemistry

In this work, microglial activation, morphology and distribution were analysed using Iba1 (Ionized calcium binding adaptor molecule), microglia cell density with Pu.1 (myeloid cell transcription factor), microglial proliferation with phosphohistone 3 (pH3), microglia phagocytosis with CD68 (lysosome-associated glycoprotein), antigen presenting activity with MHC-ll (major histocompatibility complex-class ll), astrocytes reactivity with GFAP (Glial fibrillary acidic protein), neutrophil and lymphocytes recruitment by MPO (myeloperoxidase) and CD3 (cluster of differentiation 3), respectively, and finally IgG (serum protein) for the analysis of the BBB permeability (Table1).

In all cases, sections were washed with TBS (0.05 M, pH 7.4) and TBST 0.1% (pH 7.4) and incubated in 70% methanol + 2% H_2O_2 for 10 minutes, to blocked the endogenous peroxidase reactivity. Then, sections were incubated with blocking buffer (BB) containing TBST 0.1% + 10ml FBS+0.3% BSA for 1h at room temperature (RT). In case of Pu.1, sections were firstly treated with antigen retrieval solution, containing sodium citrate buffer (pH 8.5, at 80℃ for 40′). Subsequently, sections were incubated overnight at 4℃ followed by an hour at RT with primary antibody diluted in the same BB (Table 1). Sections incubated with the same BB lacking the primary antibody were used as a negative control.

Then, sections were rinsed with TBST 0.1% and incubated with corresponding biotinylated secondary antibody for 1h at RT. After washing with TBST 0.1%, sections were incubated with horseradish peroxidase conjugated streptavidin diluted in the same BB for 1h at RT. Finally after washing with TBS and TB the immune reaction were visualized incubating sections with by 3,3-diaminobenzidine (DAB) solution (90ml TB+0.05gr DAB powder+33μl H2O2). Sections were dehydrated in graded alcohols, treated with xylene and coversliped with histology mounting media.

Densitometric Analysis

To study microglial and astrocyte reactivity, quantitative analysis of sections stained with Iba1, CD68, MHC-II and GFAP were performed. For each immunohistochemistry, a minimum of five TBI-lesioned WT and five TBI-lesioned GFAP-IL10Tg animals at 24hpi, 3 and 7dpi, as well as four NL WT and four NL GFAP-IL10Tg animals were analyzed. Five sections from each animal and time-point including two areas of interest, namely lesioned core and peri-lesional part (PLP) (Figure 3), were analyzed. Three photos of each section were captured at 20x magnification with a DXM 1200F Nikon digital camera joined to a brightfield Nikon Eclipse 80i microscope, using the ACT-1 2.20 (Nikon corporation) software. For each photograph, both the percentage of area occupied by the immunostaining (%Area) and the intensity of the immunoreaction (Mean Gray Value) were calculated using the analySIS® software. The level of immunoreactivity (AI) was calculated by multiplying the percentage of area and the intensity of immunolabeling.

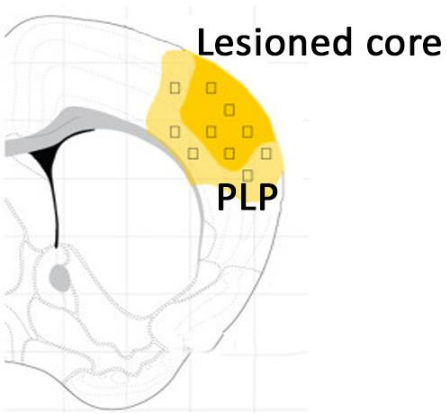

Figure 5.
Scheme illustrating the lesioned core (dark yellow) and peri-lesional part (PLP) (light yellow). Adapted from Perego et al., 2011.

For microglial cell density quantification, sections stained with Pu.1 were used. A minimum of three TBI-lesioned WT and three TBI-lesioned GFAP-IL10Tg animals at all time points, and four NL WT and four NL GFAP-IL10Tg mice were analysed. A minimum of five sections from each animal including both the lesioned core and the PLP part were analysed. Three photo of each section were captured with 10x magnification using the same device and software specified above. The number of Pu.1+ nuclei was obtained by “Automatic Cell Counter” (ITCN) plug-in from NIH Image J® software (Wayne Rasband, National Institutes of Health, USA). Data were expressed as cells/mm^2.

Quantification of microglial cell proliferation was performed on sections immunolabeled for the mitotic marker phosphohistone 3 (pH3) in both NL and TBI-lesioned animals at 24hpi, 3 and 7dpi. At least three WT and three GFAP-IL10Tg animals were analyzed. The number of pH3 positive cells was manually counted on five different sections per animal using the 20x objective. Data were averaged and expressed pH3+ cells/section.

To evaluate neutrophil migration after TBI, sections stained with MPO were used. A minimum of three WT and three GFAP-IL10Tg animals were used for each time point. At least five different sections of each animal were studied. A minimum of three photos of each section were captured by 20x magnification with a DXM 1200F Nikon digital camera joined to a brightfield Nikon Eclipse 80i microscope, using the ACT-1 2.20 (Nikon corporation) software. The number of MPO+ cells of each photo was counted using the Image J® software and data were averaged and represented as MPO+/section.

Quantification of lymphocyte infiltration was carried out on sections immunolabelled with CD3 at 3 and 7dpi after TBI. At least five WT and five GFAP-L10Tg animals were analyzed. A minimum of five different sections of each animal were captured at 20x magnification using the same device and software specified above. Data were averaged and expressed as CD3+/section.

To evaluate BBB disruption after TBI, a minimum of three WT and three GFAP-IL10Tg animals were used at 24hpi and 3dpi. At least five sections of each animal immunolabeled with IgG were studied. Each section were captured by 2x magnification at all time points and the area occupied by the IgG staining was measured. Data was averaged and expressed as μm^3.

Table 1. List of antibodies and reagents used for immunohistochemistry

Primary antibody	Iba1	Rabbit	1:1000	019-19741	Wako
	Pu1	Rabbit	1:400	2258S	Cell Signalling
	pH3	Rabbit	1:3000	06-570	Millipore
	MPO	Rabbit	1:100	9535	Abcam
	CD68	Rat	1:1000	MAC 1957	BIO-RAD
	GFAP	Rabbit	1:500	Z0334	Dako
	GFAP	Mouse	1:100	G3893	Sigma-Aldrich
	IL-10R1	Rabbit	1:50	Sc-985	Santa Cruz
	CD11b	Rat	1:100	MCA711G	AbD Serotec
	CD3	Hamster	1:250	MCA2690	AbD Serotec
	MHC-ll	Rat	1:25	TIB-120	Hybridoma supernatant ATCC
Secondary antibody	Biotinylated	Rabbit	1:500	BA-1000	Vector Laboratories
	Biotinylated	Rat	1:500	BA-4001	Vector Laboratories
	Biotinylated	Hamster	1:500	BA-9100	Vector Laboratories
	Biotinylated	Mouse	1:500	BA-2001	Vector Laboratories
	Alexa 488	Mouse	1:500	A11029	Invitrogen
	Alexa555	Rabbit	1:500	A21428	Invitrogen
Streptavidin –HRP			1:500	SA-5004	Vector Laboratories
Streptavidin-Alexa Fluor 555			1:500	S21381	Life Technologies
Streptavidin-Alexa Fluor 488			1:500	S11223	Invitrogen
DAPI			1:10,000	9542	Sigma -Aldrich

.

Double Immunofluorescence and Confocal analysis

To detect proliferative microglial cells, immunofluorescence combining pH3 and CD11b antibodies was performed. Sections were processed following the same procedure specified in the previous paragraph for pH3 staining but using anti-rabbit Alexa -Fluor® 555 conjugated antibody as a secondary antibody. Then, sections were washed with TBST 0.1% and incubated for 1 h at RT in BB and incubated with anti-rat CD11b diluted in BB overnight at 4℃ followed by and one more hour at RT. Afterwards, sections were washed with TBST 0.1% and incubated with biotinylated anti-rat secondary antibody for 1h at RT and with Alexa-Fluor® 488 conjugated streptavidin diluted in BB for an 1h at RT. At the end, sections were washed with TBST 0.1%, TBS and TB.

To determine IL-10R1 colocalization with astrocytes, double immunofluorescence using IL-10R and GFAP was performed. First, sections were dried 6h at RT, washed with TBS and TBST 0.1% and incubated for 1h at RT with the blocking buffer solution 2 (BB2), containing 0.2% gelatin (powder food grade, 104078, Merck, Burlington, Massachusetts, USA) in TBST 0.1%. Then sections were incubated with anti-rabbit IL-10R1 antibody for 48h at 4℃ followed by one more hour at RT. After washing with TBST 0.1% sections were incubated with biotinylated anti-rabbit antibody diluted in BB2 for 1h at RT. Then sections were washed with TBST 0.1% followed by incubation with Alexa-Fluor® 555 conjugated with streptavidin diluted in BB2 for 1h at RT. Sections were then washed with TBST 0.1% and incubated with BB containing 90 ml TBST 0.1%+10ml FBS+0.3gr BSA for 1h at RT. Experiment was followed by incubation with anti-mouse GFAP diluted in BB overnight at 4℃ followed by one more hour at RT. Subsequently, sections were washed with TBST 0.1% and incubated with anti-mouse Alexa Fluor® 488 diluted in BB for 1h at RT.
All double labelled sections were stained with 4,9,6-diamidino-2-phenylindole (DAPI) diluted in TB for 10 min, before being cover-slipped with Fluoromount G™ (0100-01; SouthernBiotech, Birmingham, AL). Negative controls were performed by incubating the sections with the corresponding BB but without the primary antibodies.

Flow cytometry analysis

The phenotype of microglia and monocyte/macrophage populations, in NL and TBI-lesioned animals (at 24hpi 3 and 7 dpi) were analyzed using flow cytometry as previously described (Almolda, Costa, Montoya, Gonzalez, & Castellano, 2009).

Briefly, anaesthetized animals were intracardially perfused for 1 min with 0.1M phosphate buffer solution (PBS), the brain removed and the cortex was quickly dissected out. In order to obtain a cell suspension, samples were dissociated through 140 µm and 70 µm meshes and digested for 30 min at 37ºC using type IV collagenase (17104-019, Life Technologies) and DNAsa I (D5025, Sigma). Subsequently, each cellular suspension was centrifuged at RT for 20 min at 2400 rpm in a discontinuous density Percoll gradient (17-0891-02, Amersham-Pharmacia) between 1.03 g/ml and 1.08 g/ml. Cells in the interphase and the clear upper-phase were collected, washed in PBS plus 2% serum and the Fc receptors were blocked by incubation for 10 min at 4ºC in a solution of purified CD16/32 diluted in PBS plus 2% serum. Afterwards, cells were labeled for 30 min at 4ºC with the two following combinations of surface antibodies: **1)** anti-CD11b-PE-Cy7, anti-CD45-PerCP, anti-CCR2- PE, anti-ly6c -FITC, and anti-F4/80 APC-Cy7; **2)** anti-CD11b-PE-Cy7, anti-CD45-PerCP, anti-TREM2-PE, and anti-CD68-APC (Table 2). In parallel, isotype-matched control antibodies for the different fluorochromes (BD Pharmingen) were used as negative control and a cell suspension of splenocytes as positive control. Data were extrapolated as number of cells using Cyto CountTM fluorescent beads, following the manufacturer's instructions (S2366, Dako Cytomation). Finally, cells were acquired using a FACS Canto flow cytometer (Becton Dickinson, San Jose, CA) and results analyzed using the FlowJo® software. The analysis was performed separately for each animal without any pooling.

Table 2. List of antibodies used for the flow cytometry analysis.

Target antigen		Format	Dilution	Cat number	Manufacture
Fc blocker	CD16/32	purified	1:250	553142	BD pharmingen
Primary antibody	CD11b	PE-Cy7	1:400	557657	BD pharmingen
	CD45	PerCP	1:400	557235	BD Biosciences
	CCR2	PE	1:400	150609	Biolegend
	CD68	APC	1:400	137007	Biolegend
	TREM2	PE	1:400	FAB17291P	R &D Company
	Ly6c	FITC	1:400	553104	BD Biosciences
	F4/80	APC-Cy7	1:400	123117	Biolegend

Tissue processing for protein analysis

Animals used for protein analysis were anesthetized with an intraperitoneal injection (i.p) of Ketamine (80 mg/Kg) and Xylazine (20mg/Kg). Anesthetized animals were perfused with pre-cold phosphate buffered saline (0.1M, Ph 7.4) PBS for 1 min. Then the ipsilateral part were dissected and snap frozen individually in liquid nitrogen and stored at -80ºC. Total protein was extracted by solubilisation of samples on lysis buffer containing 25mM HEPES, 2% Igepal, 5mM $MgCl_2$, 1.3mM EDTA, 1mM EGTA, 0.1M PMSF and protease (1:100, P8340, Sigma Aldrich) and phosphatase inhibitor cocktails (1:100, P0044, Sigma Aldrich) for 2 hours at 4ºC. After solubilisation, samples were centrifuged at 13000 rpm for 5 min at 4ºC and the supernatants collected. Total protein concentration was determined with a commercial Pierce® BCA Protein Assay kit (#23225, Thermo Scientific) according to manufacturer's protocol. Protein lysates were aliquot and stored at -80ºC until used for ELISA and protein microarray analysis. The hippocampus from each animal was analyzed separately.

Cytokine-Chemokines analysis

The cytokines IL-1β, TNF- α and IL-10 and the chemokines CXCL1 (KC/GRO) and CCL2 (MCP-1) were analyzed using a Milliplex® MAP Mouse Cytokine/Chemokine kit (#MCYTOMAG-70K, Merck Millipore) according to manufacturer's instructions. Briefly, 25 µL of each cortex extracts with a final total protein concentration of 3 µg/µL were added to the plates, along with the standards in separate wells, containing 25 µL of custom fluorescent beads and 25 µL of matrix solution, and incubated overnight at 4ºC in a plate-shaker (750 rpm). After two washes with wash buffer (1x), the plate was incubated with 25 µL of detection antibodies for 30 min at RT followed by incubation with 25 µL of Streptavidin-Phycoerythrin for 30 min at RT in a plate-shaker (750 rpm). Finally, the plate was washed twice with wash buffer and 150 µL of Drive fluid was added. Luminex® MAGPIX® device with the xPONENT® 4.2 software was used to read the plate. Data were analyzed using the Milliplex® Analyst 5.1 software and expressed as pg/mL of protein.

Statistical Analysis

All experimental values were expressed as mean values ± standard error of the mean (SEM). Graph Pad Prism®6 software were used for statistical analysis. Two-way ANOVA test with the Fisher's Test as a post-hoc test two compare among the groups.

Results

1. Transgene-encoded IL-10 does not make any changes in the brain cyto-architecture.

To detect possible alterations in the brain cyto-architecture induced by transgene-encoded IL10 production in the brain, a microscopic study of toluidine blue stained section was performed in both NL conditions and after TBI (Fig.6). Our analysis demonstrated no differences in the disposition and size of neuronal layers or the number of cells in the cerebral cortex between NL WT and NL GFAP-IL10Tg mice. After TBI, at 24hpi depleted area o neurons was observed in the lesion core surrounded by an area of neurons with pigmented nuclei, corresponding to the penumbra area. The number of cells in the lesion progressively increased from 3 to 7dpi, showing an area densely occupied by cells. No apparent differences between WT and GFAP-IL10Tg mice were found at any time-point analyzed in either the lesioned cavity or the penumbra areas (Fig. 6).

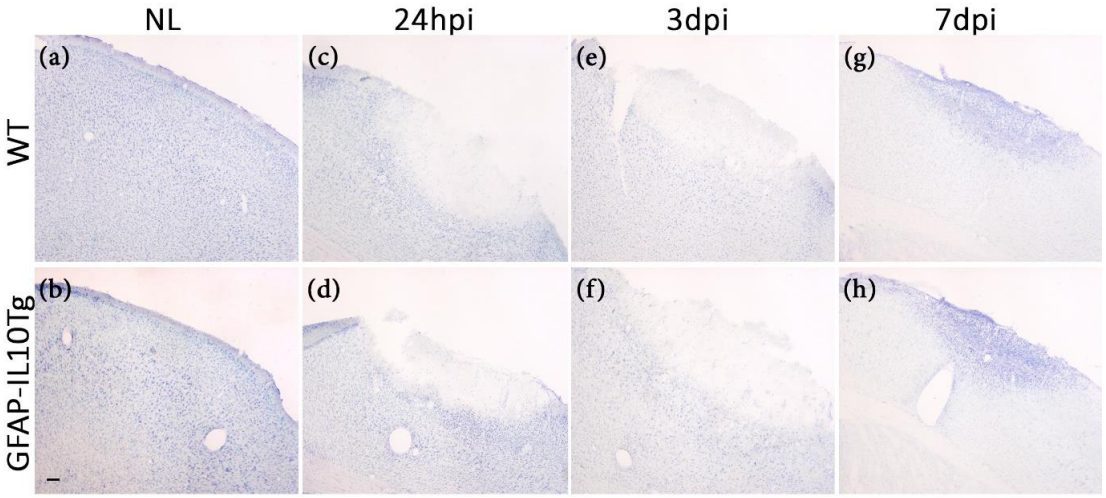

Figure 6. Toluidine blue staining. Representative images showing the toluidine blue staining of cortex in non-lesioned (NL) WT (a) and NL GFAP-IL10Tg animals (b). No detectable difference was observed in cortical cyto-architecture of NL WT and NLGFAP-IL10Tg. After TBI, both WT (c-e-g) and GFAP-IL10Tg animals (d-f-h) showed the area of lesion in the cortex characterized by a depleted area of neurons surrounded by the penumbra, exhibiting pigmented nuclei indicative of degeneration from 24hpi to 7dpi. No differences were detected between WT and GFAP-IL10Tg animals at any time point studied. Scale bar=100µm.

2. IL-10 upregulation showed a neuroprotective role at early time-points after TBI.

In order to study effect of IL-10 on neuronal degeneration, sections were stained with FluoroJade-B (FJ-B), a marker associated to degenerating neurons. FJ-B+ neurons were observed in the area just surrounding the lesion cavity, in both WT and GFAP-IL10Tg mice, with a maximum number at 24hpi and progressively decreasing from 3 to 7dpi. Although the dynamics of FJ-B was similar in both experimental groups, a significant decrease in the number of FJ-B+ cells was reported in GFAP-IL10Tg at 24hpi and 3dpi when compared with WT (Fig. 7).

FJ-B immunostained sections were also used to measure lesion size. No detectable differences in the lesion volume or the spread of the lesion were observed between WT and GFAP-IL10Tg animals at any time-point studied.

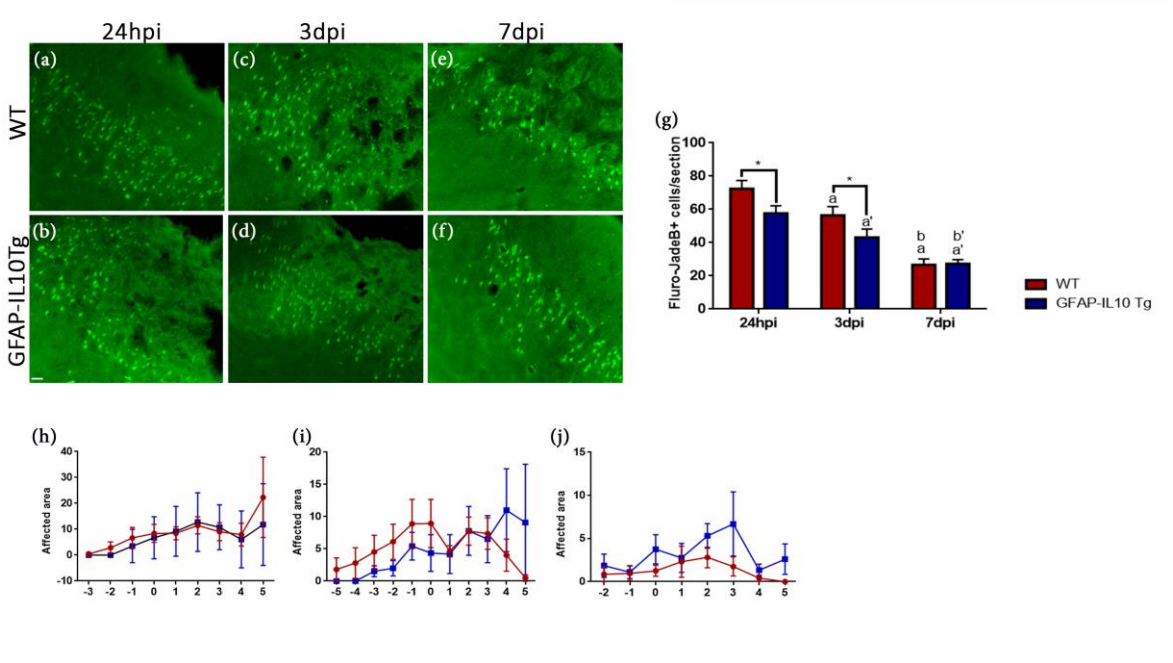

Figure 7. Fluoro-Jade B staining. Representative images revealing neuronal degeneration within the area just surrounding the lesion cavity in WT (a-c-e) and GFAP-IL10Tg animals (b-d-f). (g) Graph showing the quantification of FluoroJade-B (FJ-B)+ cells along the different time-points after TBI. Note that transgenic animals showed lower degenerating neurons in comparison to WT at 24hpi and 3dpi. (h, i, j) Graphs showing the quantification of lesion volume at 24hpi (a), 3dpi (b) and 7dpi (c) in both WT and GFAP-IL10Tg animals. No significant differences between WT and GFAP-IL10Tg animals were observed at any time points analyzed. Data are represented as mean±SEM. (*p ≤ 0.05). In WT; a indicates significance vs NL, b: indicates significance vs 24hpi. In GFAP-IL10Tg animals; a' indicates significance vs NL, b': indicates significance vs 24hpi. Scale bar=50µm.

3. Microglial cell activation and morphology.

In order to assess whether differences in neuronal degeneration were associated to modifications on microglial activation, morphology and distribution along the different time points after TBI, the Iba.1 immunohistochemistry was performed.

Our analysis demonstrated significant differences between WT and GFAP-IL10Tg animals in the expression levels of Iba1, as well as in the morphology of microglia/macrophages both in NL conditions and after TBI (Fig. 8).

A significant increase in Iba1 labelling was found in GFAP-IL10Tg animals in NL conditions compared to WT. Moreover, while in WT animals microglial cells showed the typical ramified morphology, in the cortex of transgenic animals these glial cells showed an enlargement of the cell body and thicker processes.

After TBI, we observed a progressive increase, from 3 to 7dpi, in the Iba1 immunoreactivity in the two areas analyzed (lesioned core and PLP) in both WT and GFAP-IL10Tg mice. However, the dynamics in both areas and genotypes were different. In the lesioned core, WT mice showed a progressive increase in Iba1 labelling from 3 to 7dpi whereas in the PLP this increase was only seen at 3dpi and levels remained unaltered at 7dpi. In contrast, GFAP-IL10Tg mice experimented an initial abrupt decrease of Iba1 expression at 24hpi in the lesioned core that increased afterwards at 3 and 7dpi. When compared with WT, transgenic mice showed a lower Iba1 labelling at 7dpi in the lesioned core, but no modifications in the PLP area.

To graphically represent the dynamics of microglial activation following TBI in both WT and GFAP-IL10Tg animals, the fold-changes with respect to the corresponding NL animals were calculated. This representation revealed that the upregulation of Iba1 with respect to its basal levels was less pronounced in GFAP-IL10Tg animals than in WT at all time-points analyzed.

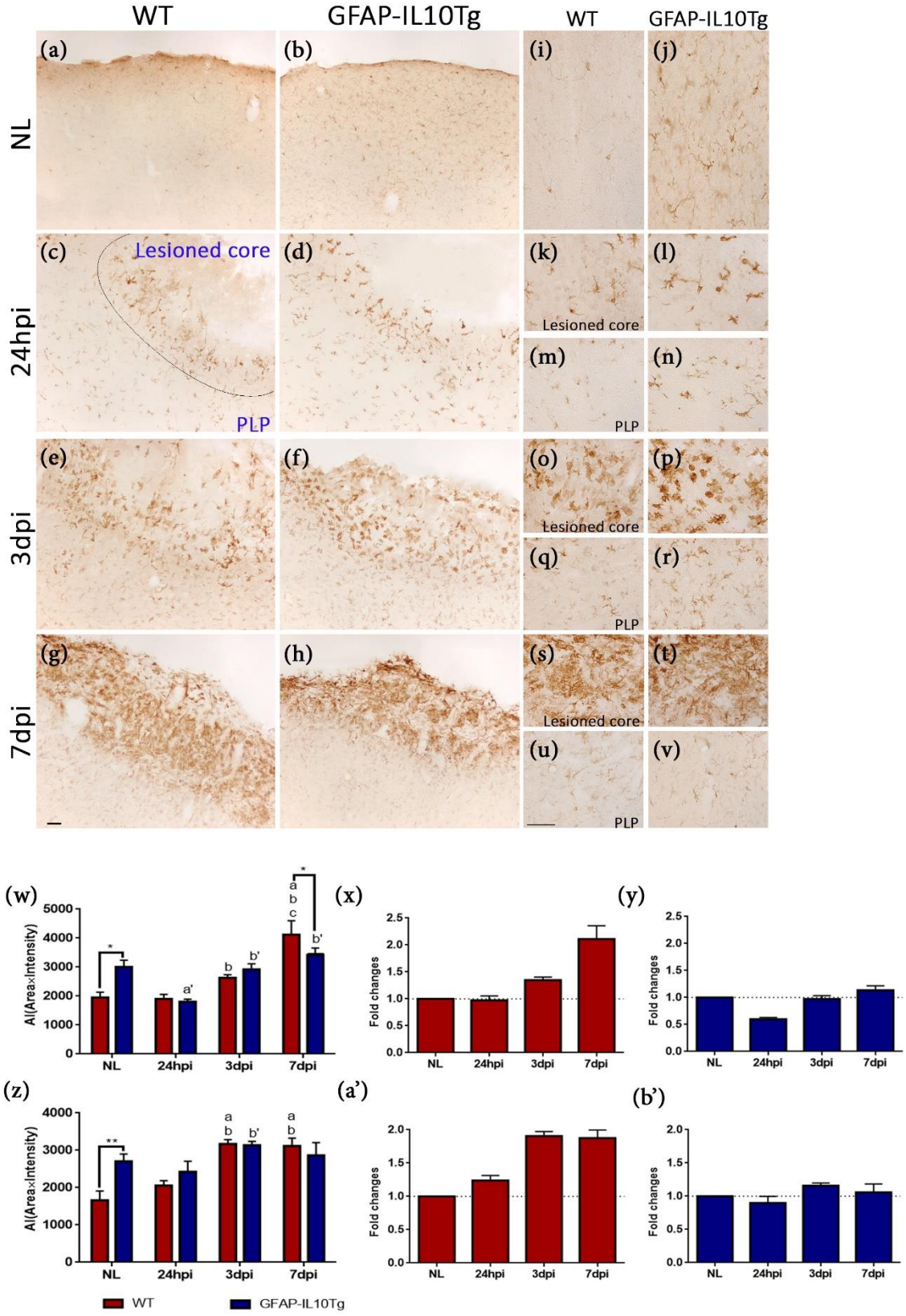

Figure 8. Iba1 immunohistochemistry. Representative images from WT and GFAP-IL10Tg animals showing Iba1 immunoreactivity in the cortex of non lesioned (NL) (a-b), and in the lesioned core of TBI-injured animals from 24hpi to 7dpi (c-h). Graphs showing the

quantification of Iba1 immunoreactivity as the AI (Area ˣ Intensity) after TBI at lesioned core and PLP. Note that microglia in NL GFAP-IL10Tg animals (w, z) showed higher Iba1 immunoreactivity than WT, associated with thicker and elongated morphologies (i, j). After TBI, a reduction of Iba labelling was observed in transgenic animals at 7dpi (w, z). Graphs showing the fold changes of Iba1 expression in comparison to the respective NL animals in WT (x, y) and GFAP-IL10Tg (a', b') animals in the affected area. GFAP-IL10Tg animals showed significant lower fold increase of Iba1 than WT in both lesioned core and peri-lesional part. All values corresponded to mean±SEM. Differences between WT and GFAP-IL10Tg animals are denoted by placing the appropriate p value above the two bars *p≤0.05. In WT animals; a indicates significant vs NL, b: indicates significant vs 24hpi, c: indicates significant vs 3dpi. In GFAP-IL10Tg animals; a' indicates significant vs NL, b': indicates significant vs 24hpi, c': indicates significant vs 3dpi. Scale bar=50µm.

In addition to variations in Iba1 immunolabelling, microglial activation was also associated with morphological modifications along the TBI lesion in both WT and GFAP-IL10Tg animals.

After TBI, in the lesioned core, activated microglia in both genotypes displayed similar morphologies depending on the time post-injury. The characteristic ramified cells with low ramifications observed at 24hpi became foamy-amoebic forms at 3dpi and elongated cell nuclei with thick and short processes at 7dpi (Fig. 8).

In the PLP part, microglia showed ramified morphologies at 24hpi, becoming bushy at 3dpi and elongated at 7dpi in both WT and GFAP-IL10Tg animals.

No differences were found between WT and GFAP-IL10Tg animals in terms of microglia distribution or morphologies in either basal condition or after TBI.

4. IL-10 induces an increase in microglial cell density in basal conditions and at 3dpi.

In order to study the effects of astrocyte-targeted IL-10 production on microglial/macrophage cell density along the different time points in the lesioned core and peri-lesional part (PLP), the immunohistochemistry for the transcription factor Pu.1 (a specific myeloid marker) was performed.

Our results showed a significant increase in the number of Pu.1 positive cells in NL GFAP-IL10Tg animals in comparison to NL WT animals (Fig. 9). After TBI, both WT and GFAP-IL10Tg animals experimented a remarkable increase in the number of Pu.1 cells, but with some disimilarities in the dynamics. While in WT, a progressive increase of Pu.1 positive cells were observed from 3dpi reaching the maximal at 7dpi in the lesioned core, in GFAP-IL10Tg animals this increase showed the maximal at 3dpi and remained stable at 7dpi. Moreover, the number of Pu.1 positive cells was two-fold higher in GFAP-

IL10Tg than in WT at 3dpi. Again, the representation of Pu.1 in terms of fold changes respect to their corresponding NL animals demonstrated that the upregulation of microglia/macrophage cell density was less pronounced in transgenic animals than in WT.

In the peri-lesional part, WT animals showed an upregulation in the number of cells at 3dpi that remained stable at 7dpi. In contrast, GFAP-IL10Tg mice showed and initial decrease in the Pu.1 positive cells at 24hpi that was not observed in WT (Fig. 9).

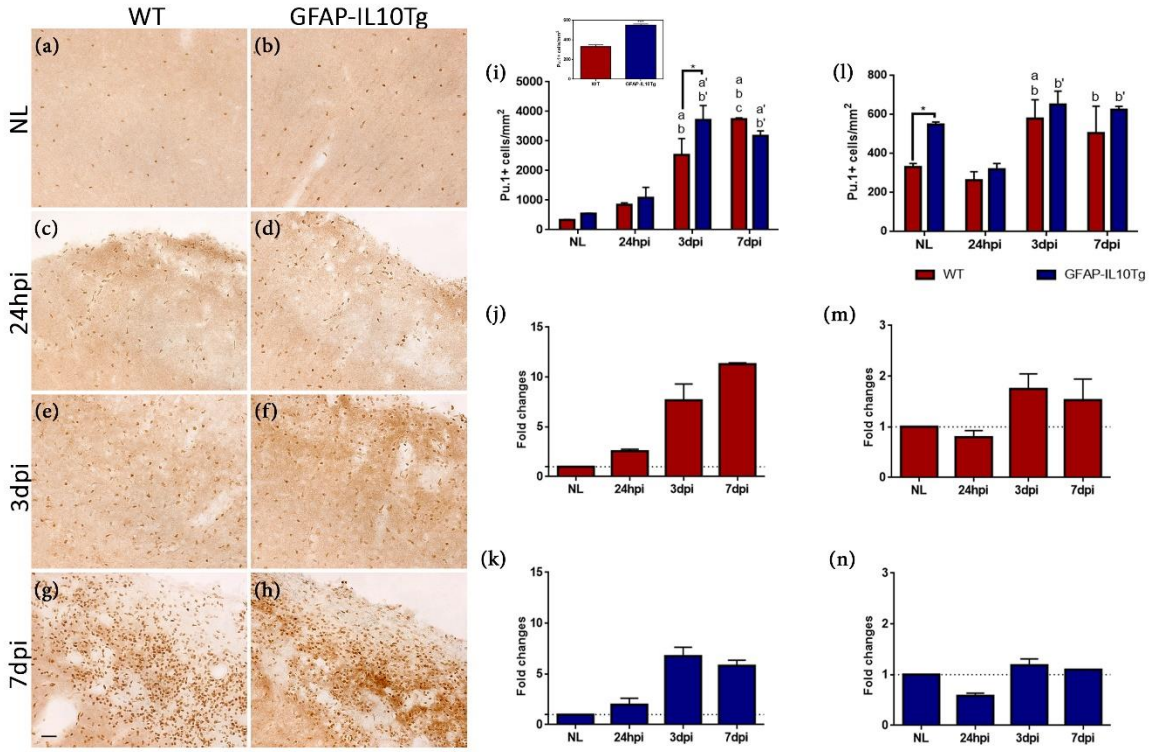

Fig 9. Pu.1 immunohistochemistry. Representative images showing the number of Pu.1 in the lesioned core of both WT (a-c-e and g) and GFAP-IL10Tg (b-d-f and h) animals. (j and l) Graphs showing the quantification of Pu.1+ cells of both WT and GFAP-IL10Tg in non lesioned and lesioned animals from 24hpi to 7dpi in the lesioned core (j) and peri-lesional part (k). Note that GFAP-IL10Tg animals showed higher number of Pu.1 + cells in NL and at 3dpi. (j,k,m,n) Graphs showing the fold change of Pu.1+ cells in WT (j, m) and GFAP-IL10Tg (k, n) in comparison to their NL animals. Note that in GFAP-IL10Tg mice the increase of Pu.1+ cells along the injury in less pronounced than in WT, specially at 7dpi in the lesioned core. All values are indicated as mean±SEM. *p ≤ 0.05. In WT animals; a indicates significance vs NL, b: indicates significance vs 24hpi, c: indicates significance vs 3dpi. In GFAP-IL10Tg animals; a' indicates significance vs NL, b': indicates significance vs 24hpi. Scale bar=30µm.

5. Transgene-encoded IL-10 induces an inhibitory role in microglia proliferation.

In order to study whether changes observed in microglial cell density were related to modifications in proliferation, sections were labelled for phospho-histone H3 (pH3) (cell proliferation marker). No pH3+ cells were found in NL WT and NL GFAP-IL10Tg animals. After TBI, both groups of animals underwent a drastic increase in the number of pH3+ cells at 24hpi. In WT animals, this increase continued until 3dpi and decrease thereafter at 7dpi. In contrast, in GFAP-IL10Tg mice, the number of pH3+ cells decreased significantly at 3dpi and remained constant at 7dpi. Thus, the number of pH3+ cells at 3dpi was significantly higher in WT animals than in GFAP-IL10Tg.

To analyze the phenotype of proliferating cells a double immunofluorescence combining CD11b (pan-microglia/macrophages marker) and pH3 (proliferation marker) was performed. Quantification of double CD11b+/pH3+ cells indicated that almost all pH3+ cells corresponded to microglia/macrophages in both WT and GFAP-IL10Tg animals and confirmed the low amount of double positive cells in transgenic animals at 3dpi (Fig. 10).

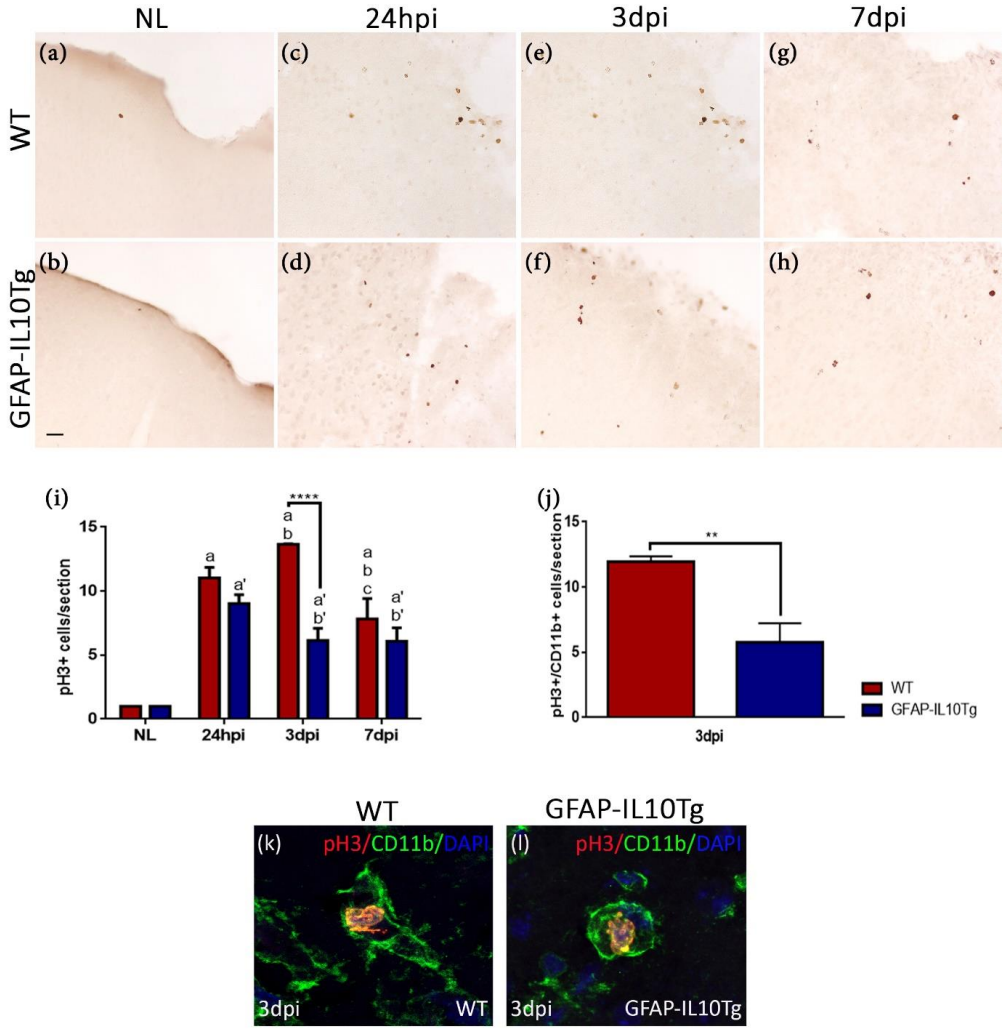

Figure 10. **Microglial/macrophages proliferation**. (a-h) Representative images showing the number of pH3 cells in the area just surrounding the lesion cavity of both WT (a-c-e and g) and GFAP-IL10Tg (b-d-f and h) animals. (i) Graph showing the quantification of pH3+ cells/section in non lesioned (NL) and lesioned animals from 24hpi to 7dpi in both WT and GFAP-IL10Tg animals. (j) Graph showing the quantification of microglia/macrophages (pH3+/CD11b+) cells/section at 3dpi in both WT and GFAP-IL10Tg animals. Note that in GFAP-IL10Tg animals the number of proliferating microglia/macrophages was significantly low compared with WT (****p ≤ 0.0001) (**p ≤ 0.01). (k-l) Representative images of double immunofluorescence of pH3 (red) and CD11b (green) at 3pi for WT (k) and GFAP-IL10Tg (l) animals. Nuclei of cells were counterstained with DAPI (blue). All data are represented as mean±SEM. In WT animals; a indicates significant vs NL, b: indicates significant vs 24hpi, c: indicates significant vs 3dpi. In GFAP-IL10Tg animals; a' indicates significant vs NL, b': indicates significant vs 24hpi.

6. Transgene expression of IL-10 increased the number of infiltrated monocytes.

Flow cytometry techniques were used to assess possible modifications in the number of microglia/macrophage populations induced by the transgenic production of IL-10. We identified the microglia/macrophage population based

on the positive CD11b expression in combination with differential expression levels of CD45 (Fig. 11). This helped in differentiating homeostatic from activated microglia as well as macrophages. Thus, ramified or homeostatic microglia was identified as CD11b+/CD45low and activated microglia as CD11b+/CD45int. Moreover, we identified the CD11b+/CD45high population, which may include highly activated microglia, monocytes, macrophages and dendritic cells. In this study, we have used the term CD11b+/CD45low/int to refer to the population of homeostatic and activated microglia jointly.

Our results showed no detectable differences in the number of CD11b+CD45$^{low/int}$ or CD11b+/CD45^{high} cell populations between NL WT and NL GFAP-IL10Tg mice (Fig. 11 a-b). However, expression levels of CD45 (mean fluorescence intensity), was higher in the CD11b+/CD45$^{low/int}$ cell population of GFAP-IL10Tg animals than in WT and lower in the CD11b+/CD45^{high} (Fig. 11).

After TBI, both WT and GFAP-IL10Tg animals experimented a significant increase in the number of both populations at 24hpi that remained unaltered at 3dpi. However, the number of CD11b+CD45high cells was significantly higher in GFAP-IL10Tg animals at 3dpi. Moreover, CD45 expression levels were higher in the CD11b+/CD45$^{low/int}$ cell population of GFAP-IL10Tg mice than in WT at all time-points after lesion, whereas it was similar between genotypes in the CD11b+/CD45^{high} cells.

As we already commented above, the population of CD11b+/CD45^{high} cells may include monocytes, a cell population highly related with the TBI progression. Therefore, a putative effect of IL-10 production on monocyte infiltration was studied in more detailed using CCR2, Ly6C and F4/80 by flow cytometry.

In NL conditions, a low amount of cells in the CD11b+CD45$^{low/int}$ (Fig11a-c) and CD11b+CD45^{high} (Fig11b-d) populations expressed CCR2 and Ly6C in both experimental groups. However, after TBI, both WT and GFAP-IL10Tg animals showed an increase in the number of CCR2+, Ly6C+ and CCR2+/Ly6C+ cells in the CD11b+CD45$^{low/int}$ (Fig11a-c) and CD11b+CD45^{high} (Fig11b-d) populations. This increase followed a similar dynamics in both groups increasing at 24hpi and remaining without significant modifications at 3dpi. Nevertheless, when compared between genotypes, we observed a significantly higher number of CD11b+/CD45^{high}/CCR2+ cells and CD11b+/CD45^{high}/CCR2+/Ly6C+ in GFAP-IL10Tg mice at 3dpi; and a higher number of Ly6C+ cells in the CD11b+/CD45$^{low/int}$ cell population in WT at 3dpi.

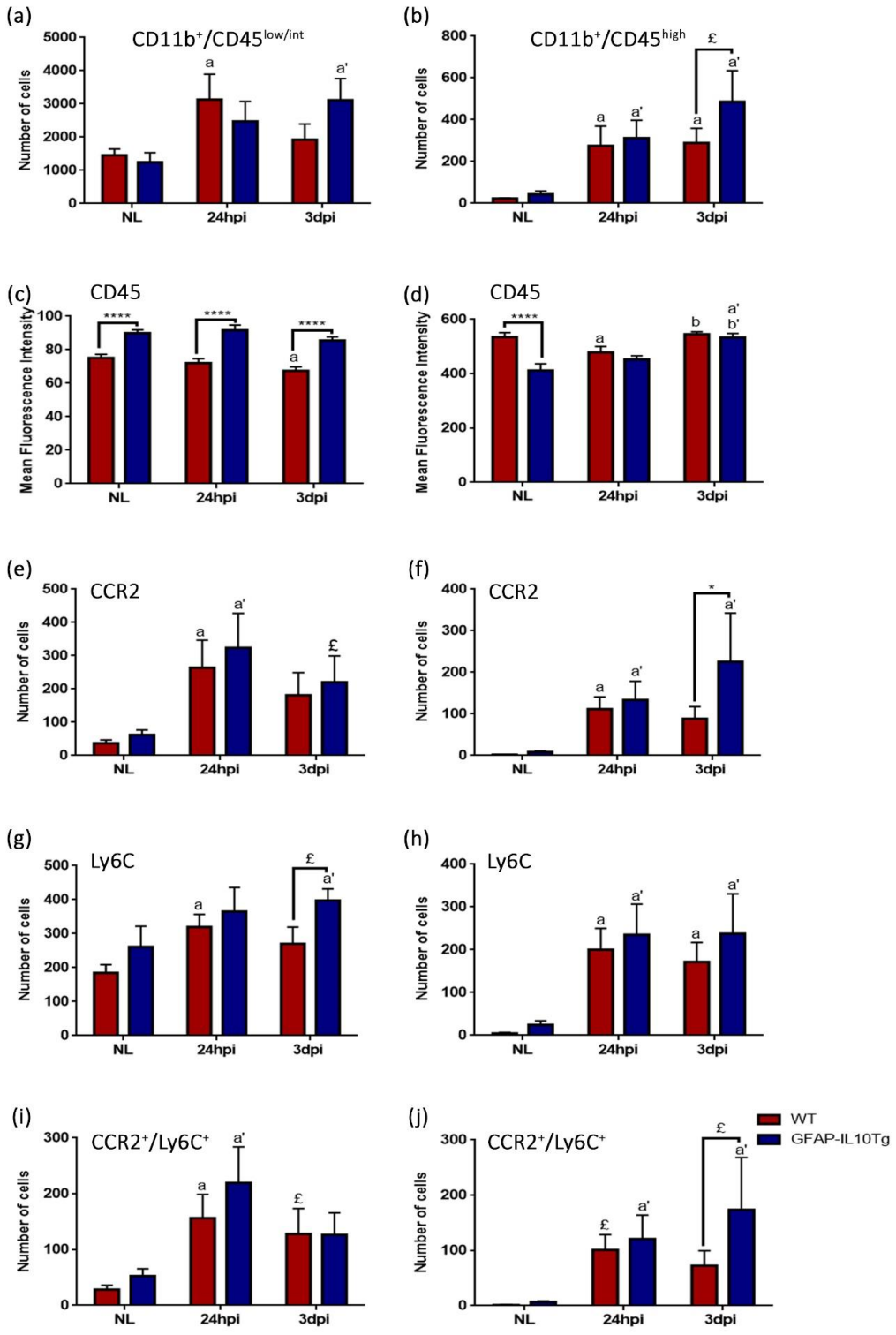

Figure 11. **Monocyte infiltration**. (a-b) graphs showing the number of cells in microglia CD11b+CD45^{low} and macrophage CD11b+CD45^{high} populations in cortex of nonlesioned (NL) and lesioned animals from 24hpi and 3dpi in WT and GFAP-IL10Tg animals. (c-d) graphs showing the intensity of CD45 in microglia CD11b+CD45^{low} and macrophage CD11b+CD45^{high} populations in of nonlesioned (NL) and lesioned animas from 24hpi to 3dpi in both WT and GFAP-IL-10Tg animals. (e-j) graphs showing Flow cytometry analysis and quantification of CCR2 and Ly6C markers in microglia and macrophage populations in nonlesioned (NL) and lesioned animals from 24hpi to 3dp in WT and GFAP-IL10Tg mice as well as quantification of monocyte recruitment.

(e-g) graphs showing the expression level of CCR2 and Ly6C in microglia CD11b+CD45^{low} (f-h) and macrophage CD11b+CD45^{high} (b-d) populations. (i-j)graphs showing the quantification of CCR2+Ly6C+ inflammatory monocytes in nonlesioned(NL) and TBI lesioned animals from 24hpi to 3dpi in WT and GFAP-IL10Tg mice. Inflammatory monocytes exhibited a significant increased in transgenic animals at 3dpi. Error bar indicates mean±SEM. (£p≤0.1,*p ≤ 0.05). In WT animals; a indicates significant vs NL, and in GFAP-IL10Tg animals; a' indicates significant vs NL.

7. IL-10 does not modify the phagocytic capacity of microglia/macrophage populations after TBI.

In order to investigate the putative changes that transgenic IL-10 production may exert on the phenotype of the microglia and macrophage cell populations both in NL and after TBI, the expression of different cell activation markers mostly related to the phagocytic function, including CD68, F4/80 and TREM2 was studied by flow cytometry in the CD11b+CD45$^{low/int}$ and CD11b+CD45^{high} populations (Fig. 12) and by immunohistochemistry (Fig. 13).

In NL conditions, the number of CD68+, TREM2+ and F4/80+ cells in both CD11b+/CD45$^{low/int}$ and CD11b+/CD45^{high} cell populations was similar in WT and GFAP-IL10Tg mice.

After TBI, the number of CD68 and TREM2 experimented a progressive increase from 24hpi to 3dpi in the population of CD11b+/CD45^{high} cells but remained unaltered in the population of CD11b+/CD45$^{low/int}$ cells. Similarly, the number of F4/80+ cells augmented at 24hpi and remained stable at 3dpi, but only in the population of CD11b+/CD45^{high} cells. No significant modifications between WT and GFAP-IL10Tg animals were detected by flow cytometry in the number of any of these cell populations.

However, when we analyzed the distribution of these cells using immunohistochemistry, we found a significant increase in the CD68 expression in the microglia/macrophages of GFAP-IL10Tg animals at 3dpi. Moreover, the analysis of fold changes for this marker, demonstrated that similarly to the resuts obtained for Iba1 and Pu.1, even the increase in the number of CD68+ cells, the upregulation of this marker in GFAP-IL10Tg animals in comparison to their NL conditions, was less pronounced than in WT (Figure 13).

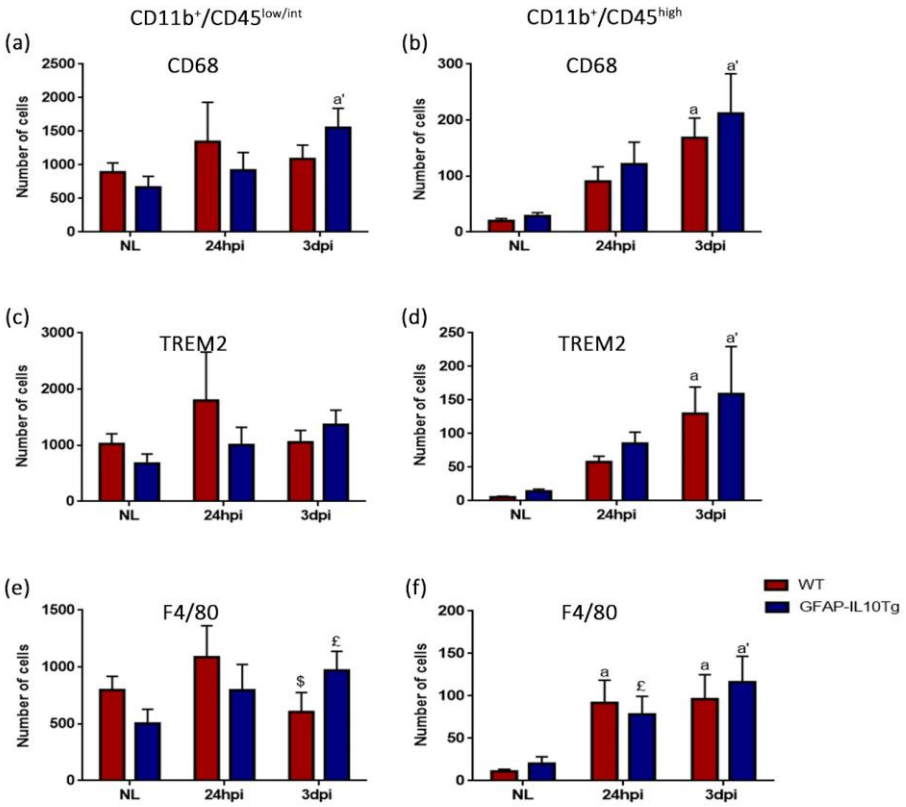

Figure 12. Microglial phagocytosis phenotype. (a-b) Graphs showing the number of cells in the microglia CD11b+CD45^{low} and macrophage CD11b+CD45^{high} populations in the cortex of nonlesioned (NL) and lesioned animals at 24hpi and 3dpi in WT and GFAP-IL10Tg animals. (c-h) Graphs showing the expression of CD68, TREM2 and F4/80 in microglia CD11b+CD45^{low} (c-e-g) and macrophage CD11b+CD45^{high} (d-f-h) populations in nonlesioned (NL) and lesioned animals at 24hpi and 3dpi in WT and GFAP-IL10Tg animals. Error bar indicates mean±SEM. (£,$ p≤0.1). In WT animals; a indicates significant vs NL, and in GFAP-IL10Tg animals; a' indicates significant vs NL.

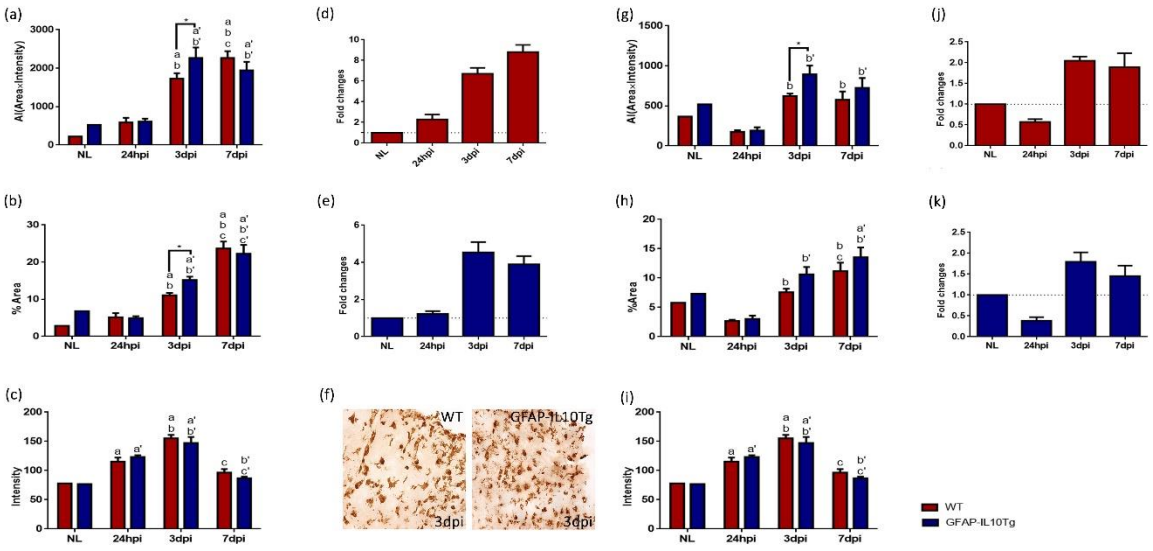

Figure 13. CD68 immunohistochemistry. (a-c and g-i) Graphs showing the quantification of CD68 immunoreactivity as the AI (Area x Intensity) (a, g), the percentage of Area (b, h) and the Mean Grey value (c, i) at lesioned core (a-c) and PLP part (g-i). Note that GFAP-IL10Tg animals showed higher expression of CD68 at 3dpi in both areas. (d-e and j-k) Graphs showing the fold changes of CD68 expression in comparison to respective NL animals in WT (d-e) and GFAP-IL10Tg animals (j-k) in the lesioned core and PLP. GFAP-IL10Tg animals showed a significant lower fold increase of CD68 than WT in both lesioned core and PLP. (f) Representative images from WT and GFAP-IL10Tg animals showing CD68 immunoreactivity in lesioned core at 3dpi. All the values are represented as mean±SEM. *p≤0.05. In WT animals; a indicates significant vs NL, b: indicates significant vs 24hpi, c: indicates significant vs 3dpi. In GFAP-IL10Tg animals; a' indicates significant vs NL, b': indicates significant vs 24hpi, c': indicates significant vs 3dpi.

8. Transgene-encoded IL10 does not make any changes in microglia antigen -presenting activation.

In order to assess the effects of astrocyte-targeted IL10 production on the microglia antigen presenting characteristics after TBI, sections were immunolabeled for major histocompatibility complex-ll (MHC-ll) at all time points of studied. No expression of MHC-ll was detected in microglial cells of NL WT or NL GFAP-IL10Tg animals. After TBI, in WT animals, MHC-ll staining appeared at 24hpi in activated microglia showing bushy and elongated morphologies in the PLP area and remained stable at 3dpi. After that, MHC-ll staining progressively augmented at 7dpi in the same area. No significant differences in either the dynamics or the morphology of MHC-II+ cells were found between WT and GFAP-IL10Tg animals at any time points analyzed (Figure 14).

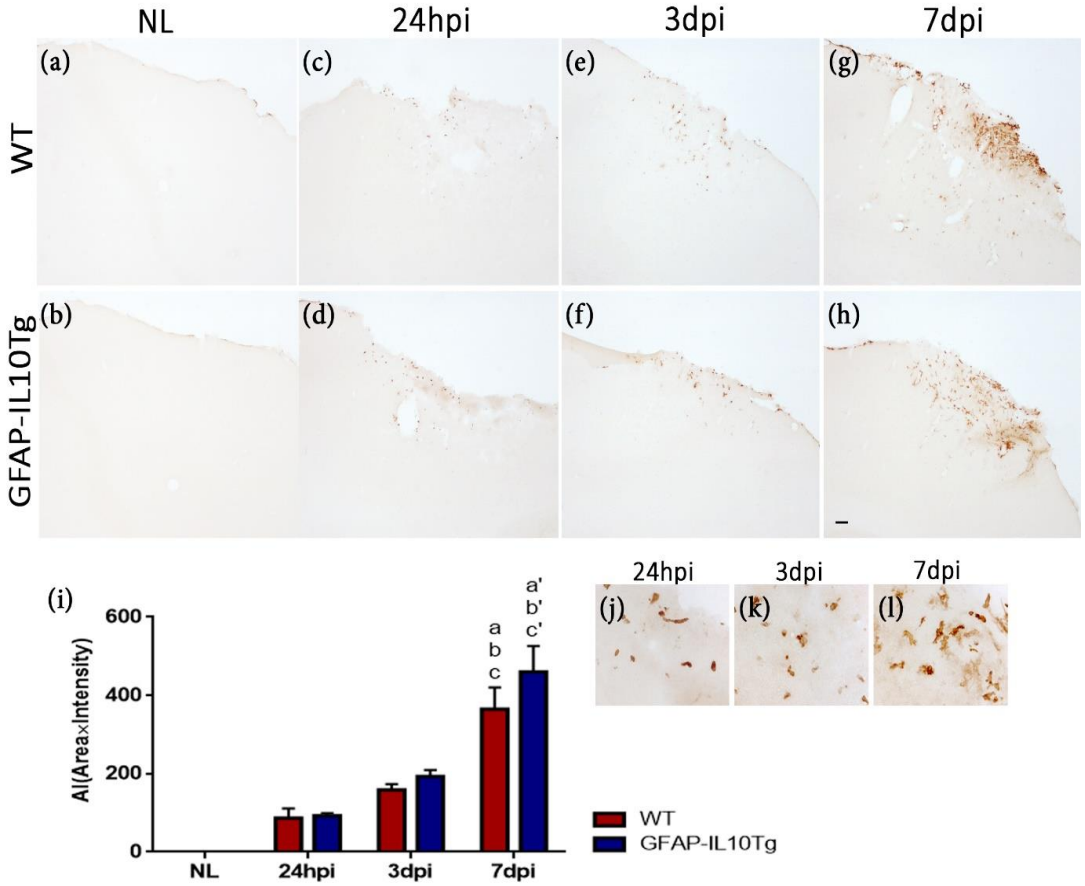

Figure 14. MHC-II immunohistochemistry. Representative images from WT (a, c, e and g) and GFAP-IL10Tg (b, d, f and h) animals showing MHC-II staining in the adjacent area to lesion core (penumbra) from 24hpi to 7dpi. Note that, MHC-II immunoreactivity was not detected at NL animals (a-b). (j-k-l) representative images exhibiting similar MHC-II morphology (rounded and elongated microglia)between WT and GFAP-IL10 animals at different time points. Scale bar=100µm.(i) graph showing the quantification of MHC-II expression as AI(Area^{x} Intensity) in both WT and GFAP-IL10 Tg animals after injury. All the values are mean±SEM. Inter-comparison statistics presented by symbol, in WT animals; a indicates significant vs NL, b: indicates significant vs 24hpi, c: indicates significant vs 3dpi. In GFAP-IL10Tg animals; a' indicates significant vs NL, b': indicates significant vs 24hpi, c': indicates significance vs NL WT. vs 3dpi

9. Transgenic production of IL-10 modified the infiltration of peripheral immune cells.

The next step we addressed was to analyze whether transgenic expression modifies the infiltration of peripheral immune cells, key components of the inflammatory response associated to TBI. Both neutrophils and T-cells were

analyzed using myeloperoxidase (MPO) and CD3/CD4, respectively, by flow cytometry and immunohistochemistry.

-Neutrophil recruitment:

No MPO+ cells were observed in NL WT or NL GFAP-IL10Tg animals. After TBI, MPO+ cells appeared at 24hpi in both WT and GFAP-IL10Tg animals, decreasing significantly at 3dpi. The number of MPO+ was significantly lower at 24hpi in transgenic mice (Figure 15).

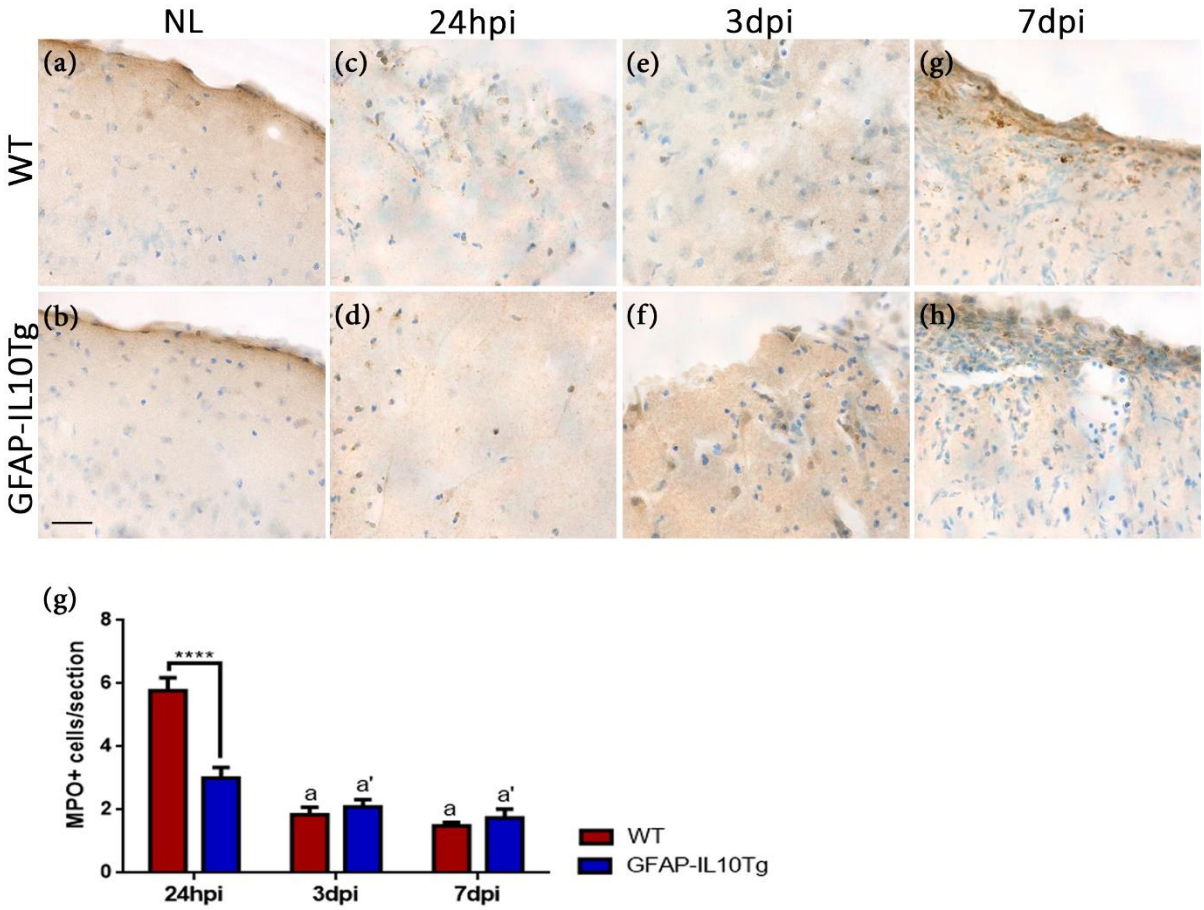

Figure 15. Neutrophils infiltration. Representative images showing the number of myeloperoxidase (MPO)+ cells (brown) in the PLP area of both WT (a-c-e and g) and GFAP-IL10Tg animals (b, d, f and h) from 24hpi to 7dpi. Toluidine blue staining was used as a nuclei marker. (g) Graph showing the quantification of MPO + cells of WT and GFAP-IL10Tg animals from 24hpi to 7dpi. Note that, at 24hpi, GFAP-IL10Tg animals presented significantly lower number of MPO+ cells in than WT. All values are represented as mean±SEM. ****p ≤ 0.0001. In WT, a: indicates significant vs NL. In GFAP-IL10Tg, a': indicates significance vs NL. Scale bar=30µm.

-Lymphocyte Infiltration

No CD3 positive cells were detected in either NL WT or NL GFAP-IL10Tg animals as well as in the contralateral side at any time points analyzed (data

not shown). After TBI, CD3 positive lymphocytes were detected and accumulated in the penumbra of ipsilateral side in both WT and GFAP-IL10Tg animals. CD3 positive cells appeared at 3dpi and remained stable at 7 dpi. There was almost two-fold increase in the total number of CD3+ cells at 3dpi in GFAP-IL10Tg when compared with WT (Fig 16).

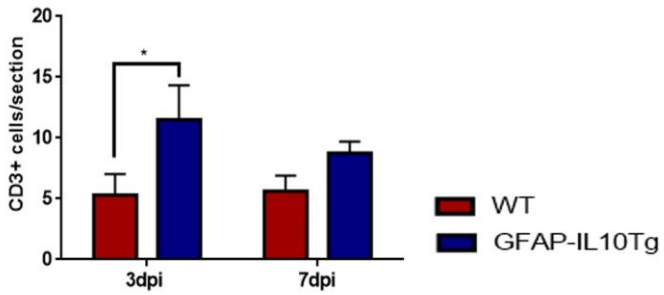

Figure 16. Analysis of T-cells. Graph showing the quantification of CD3 + T-lymphocytes in WT and GFAP-IL10Tg animals at 3 and 7dpi. Remark that, GFAP-IL10Tg presented higher number of CD3+ lymphocytes at 3dpi than WT. All the values are represented as mean±SEM. *p ≤ 0.05.

10. Blood brain barrier permeability.

In order to evaluate the possibility that the modifications in the infiltration of peripheral immune cells, observed in transgenic animals, was linked to modifications in the permeability of the blood brain barrier, immunoglobulin detection was used (Figure 17). IgG immunostaining was not detected in NL WT and NL GFAP-IL10Tg animals. After TBI, in WT animals, IgG staining was clearly observed within the lesion core and diffused into areas surrounding the primary injury at 24hpi and 3dpi. The strong leakage of IgG was observed at 24hpi followed with a significant decrease at 3dpi. In contrast to WT, in GFAP-IL10Tg animals IgG staining was remarkably low at 24hpi and remained unaltered at 3dpi.

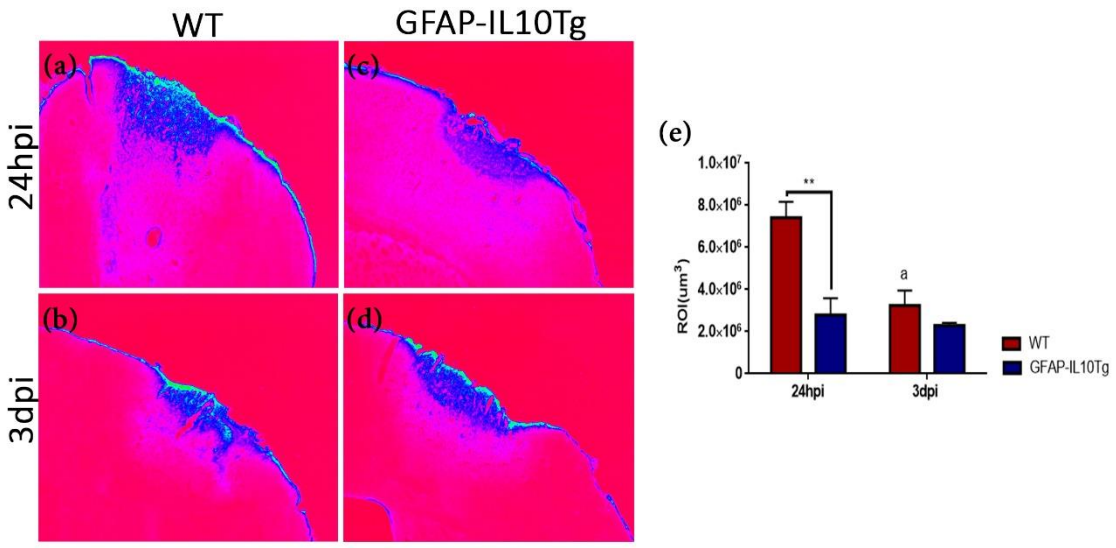

Figure 17. IgG immunohistochemistry. IgG staining was undetectable in NL of both WT and GFAP-IL10Tg animals. Representative images showing IgG immunostaining (Pseudocolor Tecnhique modified by LUT in image J software) representing BBB-leakage in WT (a-b) and GFAP-IL10Tg (c-d) animals at 24hpi and 3dpi. Blue staining represented IgG staining whereas red represented no-stained area. (e) Graph showing the quantification of volume (ROI) for IgG staining widespread in WT and GFAP-IL10Tg animals at 24hpi and 3dpi. Note that transgenic animals presented significantly lower IgG extravasation in comparison to WT at 24hpi. All the values are represented as mean±SEM. **p ≤ 0.001. In WT, a indicates significant vs 24hpi.

11. Transgene-encoded IL10 modifies GFAP expression in astrocytes.

To analyze putative differences in astrocytes, GFAP marker was used. Both NL WT and NL GFAP-IL10Tg animals showed low levels of GFAP expression. After TBI, in WT mice, GFAP staining increased abruptly at 3dpi remaining unaltered at 7dpi. In contrast, GFAP levels in GFAP-IL10Tg mice progressively increased from 3 to 7dpi, showing the maximum level at this later time-point. Thus, when compared between genotypes, levels of GFAP staining were lower in GPAP-IL10Tg animals at 3dpi in both the lesion core and the PLP area, becoming similar at 7dpi (Figure 18).

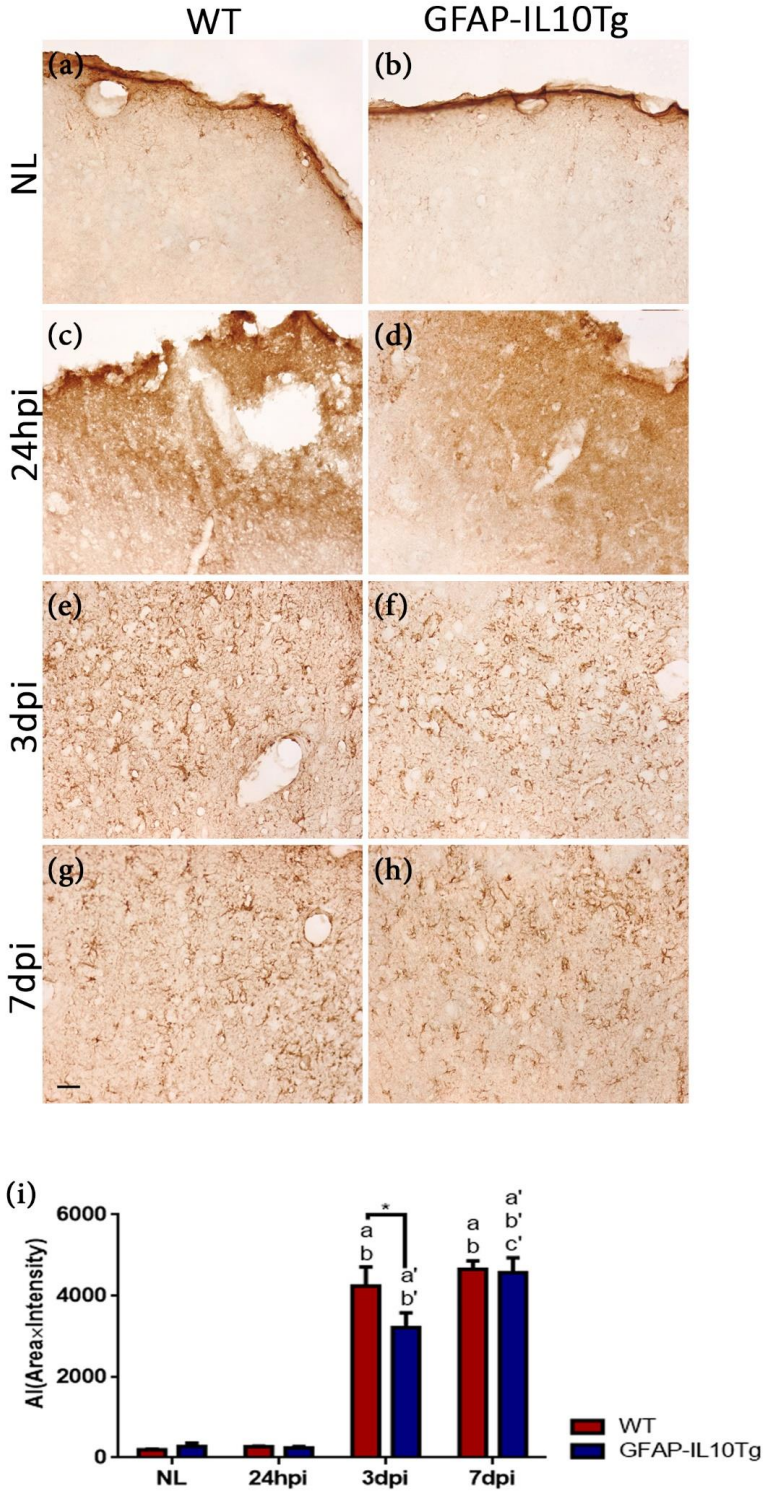

Figure 18. GFAP immunohistochemistry. Representative images showing GFAP immunostaining in the lesioned core of WT (a, c, e and g) and GFAP-IL10Tg animals (b, d, f and h) from 24hpi to 7dpi. (i) Graph showing the quantification of GFAP immunoreactivity as the AI (Area^{x} Intensity) along the lesion. Note that GFAP-IL10Tg animals presented lower GFAP labelling at 3dpi compared to WT in both the lesion core and the PLP area. All values are represented as mean±SEM. *p ≤ 0.05. In WT animals; a indicates significant vs NL, b: indicates significant vs 24hpi. In GFAP-IL10Tg animals; a' indicates significant vs NL, b': indicates significant vs 24hpi, c': indicates significant vs 3dpi. Scale bar=30µm.

12. Transgenic IL-10 production decreases the expression of IL-1β after TBI.

We address whether all the modifications observed in microglia/macrophages activation, astrocyte reactivity and leukocyte infiltration were due by changes induced by transgenic production of IL-10 in the cytokine/chemokine microenvironment generated after TBI. We specifically analyzed the expression of key cytokines associated to this kind of injury such as IL-1β, TNF-α and IL-10 and chemokines such as CXCL1 and CCL2 related to the recruitment of neutrophils and monocytes, respectively.

Our results showed a significant increase in the expression of IL-1beta and IL-10 at 4hpi in both WT and GFAP-IL10Tg that remained without significant modifications at 12hpi and 24hpi. Noticeably, transgenic animals showed a significant decrease of IL-1beta at 24hpi in comparison to WT. Regarding IL-10, although levels of expression in transgenic animals were higher at 4hpi and 12hpi, values did not reach statistically significance.

In regard of chemokines, both CXCL1 and CCL2 showed an increase at later time-points than cytokines, i.e at 12hpi decreasing thereafter at 24hpi in both genotypes. No significant differences were found between WT and GFAP-IL10Tg in any of these chemokines at any time-point analyzed (Figure 19).

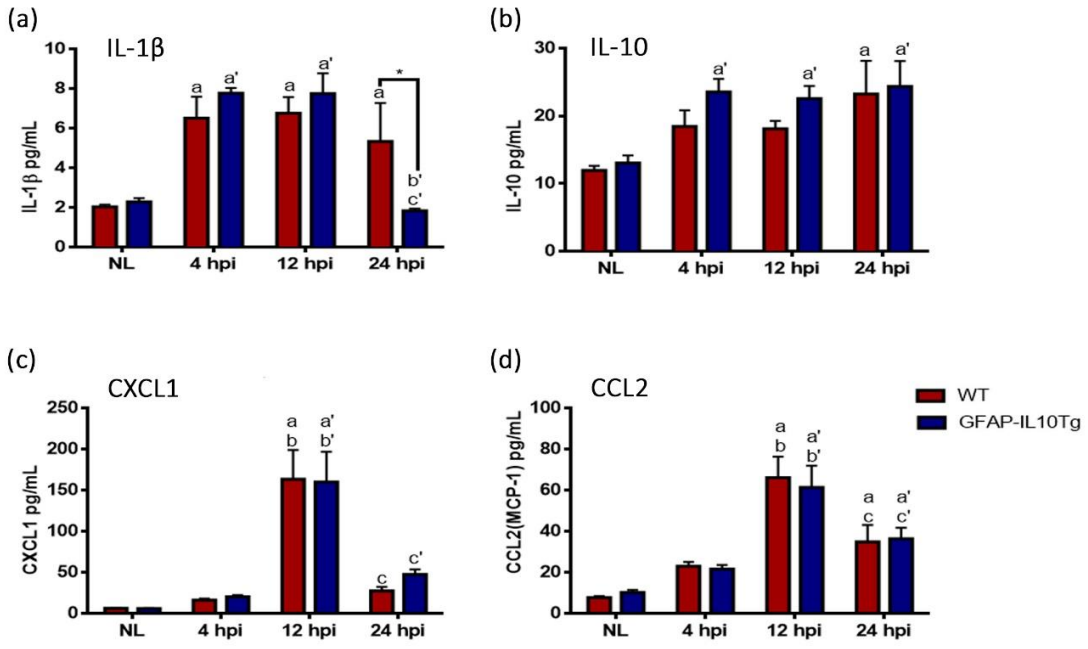

Figure 19. Cytokine/chemokine expression. Graphs showing the temporal expression of IL-1β (a), IL-10 (b) ,CXCL1 (c) and CCL2 (d) in non-lesioned (NL) and TBI-lesioned animals from 4hpi to 24hpi in both WT and GFAP-IL10Tg animals. All values are represented as mean±SEM. *p≤0.05. In WT animals; a indicates significant vs NL, b: indicates significant vs 4hpi, c: indicates significant vs 12hpi. In GFAP-IL10Tg animals; a' indicates significant vs NL, b': indicates significant vs 4hpi, c': indicates significant vs 12hpi.

13. Astrocytes are the principal cells expressing the IL-10 receptor (IL-10R) in both NL and after TBI.

Finally, in order to study which cells were responding to the transgene production of IL-10, the IL-10 receptor (IL-10R) expression was analyzed in both basal conditions and after TBI using double immunofluorescence. In NL conditions, both WT and GFAP-IL10Tg animals showed expression of IL-10R in few GFAP+ cells randomly distributed along the cortex. After TBI, IL-10R+/GFAP+ cells increased in both WT and GFAP-IL10Tg animals and were specifically located in the area just surrounding the lesion cavity. No detectable differences in the number of double positive cells were found between genotypes.

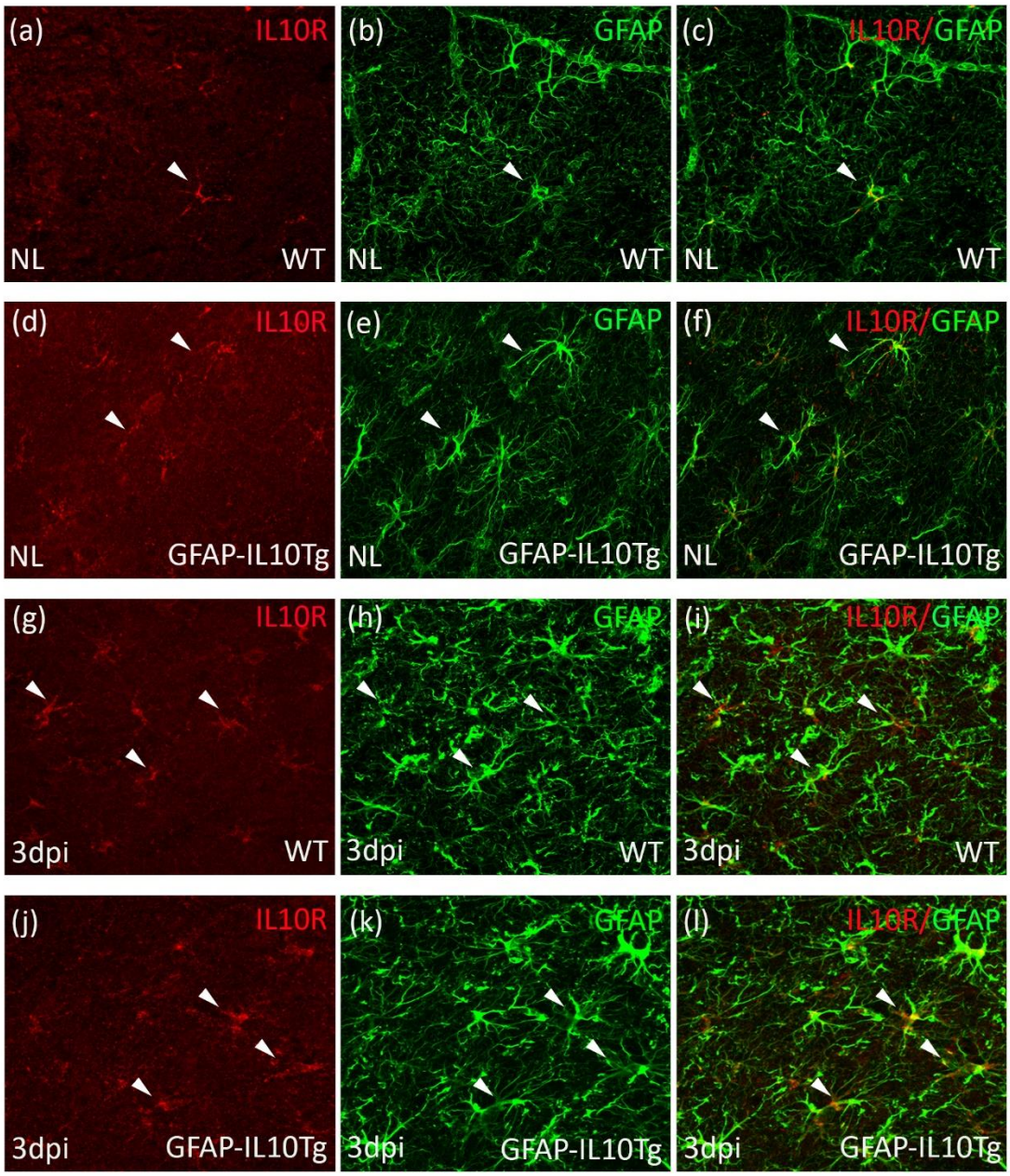

Figure 20. IL-10R expression. Representative images showing the double immunofluorescence staining for IL-10R (red) and GFAP (green) in non-lesioned (NL) (a-f) and TBI-lesioned animals (g-l) at 3dpi. Sections were counter-stained using DNA-binding DAPI (shown in blue). Note that major part of IL-10R+ cells showed co-localization (yellow) with GFAP in both NL and after TBI (arrowheads).

Discussion

With the work o this PhD we have characterized the effects of IL-10 on the neuronal degeneration, glial activation and leukocyte infiltration associated to the inflammatory response after traumatic brain injury (TBI). Our results demonstrated that IL-10 has a temporal neuroprotective role after TBI, associated to an increase in the microglia/macrophages density and modifications in their phenotype including a higher phagocytic capacity. Moreover, IL-10 production reduces the leakage of the BBB associated to trauma reducing the infiltration of neutrophils at the early time-points, but increasing the recruitment of T-cells. All these modifications were associated with a less inflammatory environment characterized by a low amount of IL-1β.

1. Transgene-production of IL-10 reduces the neurodegeneration associated to TBI.

Neurodegeneration is the principal cause of disability after traumatic brain injury. This neurodegeneration become from both primary or secondary injury. Primary injury occurs at the time of impact causing a direct damage to neural tissue, whereas by contrast, secondary injury develops in minutes to months following the insult. This secondary injury was mediated by several factors including free radical production, excitotoxicity as well as the neuroinflammatory response associated to TBI (Jassman et al., 17).

Injured neurons appeared in the ipsilateral cortex surrounding the impact site, hippocampus and thalamus. Degenerating neurons were maximal by 1 and 3 days in the cortex and hippocampus and by 7 days in the thalamus (Sato and Chang et al., 2001; Clark and Kochanek et al 1997; Conti et al., 1998; Fox and Fan et al., 1998).

Our results demonstrated neuroprotective effect of IL-10 following TBI with significant decreasing in the number of degenerating neurons at early time-points. These results are in agreement with previous published papers of our research group demonstrating the neuroprotective effects of astrocyte-targeted production of IL-10 after facial nerve axotomy (Villacampa et al., 2105) and the increase in axonal sprouting after perforant pathway transection (Recasens et al., 2019). Similarly, some studies have been reported the anti-inflammatory and neuroprotective properties of systemic administration of IL-10 after traumatic brain injury (Bethea et al., 1999; Knoblach and Faden et al 1998) and stroke (Spera et al., 1998). One possible explanation is that IL-10 exerts a direct protective effect over neurons, as in our study neurons located in the area surrounding the lesion cavity, where the neurodegenerating FJ-B+ cells were found, are the cells that presented the IL-10R1. However, we cannot discard the possibility that the positive effect exerted by IL-10

may be due to an indirect effect associated to astrocytes, as we also found expression of the IL-10R1 on astrocytes located in the same area as neurodegenerating neurons.

2. Astrocyte-targeted production of IL-10 increase microglia/macrophages cell density by promoting high monocyte recruitment.

TBI is associated with a rapid reactive response including an increase in the number of microglia/macrophages cells (Susarla et al., 2104). In concordance, our results showed a progressive increase in microglia/macrophage cell density in the cortical lesioned core and PLP after TBI in both WT and GFAP-IL10Tg animals but with some dissimilarities. GFAP-IL10Tg showed a higher cell density than WT especially at 3dpi, suggesting that overproduction of IL-10 has a role in the mechanisms underlying this increase after TBI.

Microglial proliferation has been proposed as the main mechanism mediating microglia/macrophages expansion after TBI **(**Susarla et al., 2104). As already reported, microglia/macrophages increase takes places between 3-5 days after TBI. In agreement, our results revealed that the peak of proliferative pH3+ microglia cells was observed at 3dpi in WT animals. However, correlating with the lower-fold increase reported in these transgenic mice in terms of Iba1 and Pu.1, the total number of mitotic cells in GFAP-IL10Tg animals decreased. Although initially it seems paradoxical, as GFAP-IL10Tg showed higher number of microglia/macrophages cells, it is important to take into an account here that the amount of cells in NL conditions is already higher in transgenic animals. These results pointed to IL-10 as a suppressive factor for microglial proliferation. However, IL-10 has not shown any direct effect on microglial proliferation *in vitro* (Strle et al., 2002, Sawada et al 1999) or *in vivo* after perforant pathway transection (Recasens 2019), making us to hypothesize that the effects observed in microglial cells are in fact indirect effects derived from the IL-10 actions over degenerating neurons and astrocytes, the principal cells expressing the IL-10R1 rather than on microglial/macrophages cell number. Although according to our results prevention of microglial proliferation coincided with a better outcome of TBI, suggesting a possible beneficial effect, the role of microglial proliferation after TBI is not well understood (Jassman'17). The few studies analyzing the effects of the elimination of proliferating microglia show that after TBI did not alter the extent of axonal injury (Bennet and Brody, 2014). Further studies are thus needed to demonstrate whether this proliferation is a positive or a negative event in the progression of TBI.

In addition to proliferation, modifications in the monocytes/macrophages recruitment could be another possibility to explain the increased microglia/macrophage cell density induced by IL-10. Inflammatory monocytes/macrophages has been described as the major recruited peripheral immune cells between 3 and 5 days after TBI (Rhodes et al 2014; Holmin et al 1995: Soares et al 1995: Hsieh et al 2013). In agreement, our results clearly showed a higher number of $CCR2^{+}/Ly6C^{+}$

inflammatory monocytes in the $CD11b^{+}/CD45^{high}$ cell population of both experimental groups. However, the number of recruited inflammatory monocytes was higher in GFAP-IL10Tg animals at 3dpi, coinciding with the time-point in which maximal differences between WT and transgenic mice were detected in terms of microglia/macrophages cell density. This indicates that IL-10 is influencing the recruitment of these peripheral cells. In line, we have already demonstrated that, after perforant pathway transection, astrocyte-targeted production of IL-10 promoted monocyte infiltration to the site of injury leading to an increase in the density of microglia/macrophages by modifying the profile of chemokines (Recasens et al., 2019). However, in contrast to this previous study, in this work we did not detect differences in the amount of MCP-1, the principal chemokine involved in the recruitment of monocytes between WT and transgenic animals, at least at the early time-points we measured.

3. Production of IL-10 increases microglial/macrophage phagocytic capacity but has not influence on its antigen presentation capacity.

In addition to modifications in the microglial/macrophage density, our work also demonstrated changes in the phenotype of these cells after TBI. It is well described that after acute brain injury microglial cells are rapidly activated and undergo dramatic morphological and phenotypic changes (Donat et al. 2017). The process is accompanied by the expression of surface antigens and production of mediators that build up and maintain the inflammatory response of the brain tissue (Loane et al 2014). In our present study, local production of IL-10 downregulated Iba-1 expression in activated microglia during injury evolution, supporting the previous reports that described a downregulatory effect of IL-10 on microglial activation (Norden et al., 2014, Sawada et al., 1999). However, it is clear that activation of microglia/macrophages is not a heterogenous phenomenon, but rather different phenotypes and functions have been reported for this cell population that could be relevant in the progression of the neuroinflammatory response associated to TBI (Ransohoff et al., 2016; Sica and Mantovani et al., 2012).

One of the main functions of microglia/macrophage after TBI is the phagocytosis. Microglial removal of damaged cells is a very important step in the restoration of the homeostasis and then for the recovery of the tissue after trauma. For this purpose, both CD68, a molecule located on the lysosomes, and TREM2, a molecule commonly associated with lipid recognition and phagocytosis, were analyzed. Our results demonstrated few differences in the number of CD68+ or TREM2+ microglia/macrophages cells in GFAP-IL10Tg animals compared to WT after TBI, suggesting that IL-10 was not directly modifying the phagocytic capacity of microglia/macrophages. However, when we studied in detail just the lesioned area, using immunohistochemistry, instead flow cytometry, we found an increase in CD68 labelling specifically in the lesioned area. The increase in the phagocytic capacity

of these cells in the lesioned area observed in transgenic animals, together with the lower neurodegenerative neurons found, suggested a beneficial effect of IL-10 mediated by a more rapid elimination of neuronal and tissue debris by microglia/macrophages.

Surprisingly, although IL-10 has been associated with an inhibitory effect on microglia/macrophages MHC-ll expression (Mizuno et al., 1994, Moore et al., 2001), in our work, transgenic animals did not showed alterations of MHCII, another phenotypic marker analysed, at any time points after TBI, suggesting that the antigen presenting capacity of microglia/macrophages were not altered by IL-10 in our paradigm. In agreement some studies have been described that IL-10 has no effect on MHC- II expression on Epstein-Barr virus-infected lymphoid cell lines, Langerhans cells, or activated B cells (de Waal Malefyt et al., 1991, Enk et al., 1993, Fluckiger et al., 1993).

As we will discuss in detail on the last paragraph of this discussion, the modifications observed in microglia/macrophages presumably are a result of an indirect effect mediated by astrocytes rather than a direct effect of IL-10 over microglia/macrophages population itself, because microglia/macrophages did not presented the IL-10R1 in neither NL conditions or after TBI.

4. Decreased in blood brain barrier impairment and neutrophil recruitment in transgenic animals.

Blood-brain barrier disruption has been demonstrated in the acute phase after several animal models of TBI (Habgood et al., Lotocki et al ., 200; Dietrich et al., 1994, Povlishock et al., 1978). Alterations in blood brain barrier (BBB) permeability may contribute to secondary tissue damage by the abnormal recruitment of blood components into the injured brain influencing neuronal vulnerability (Stahel, and Shohami et al., 2000; Lucas et al., 2006, Dietrich et al., 1994). These alterations in permeability occur around 3–6 hours post injury and remain visible for a longer time points at 4 and even 7 days after TBI (Habgood et al., 2007, Lotocki et al., 2009). Initial injury induces damage into vascular cell membranes leading to endothelial cells necrosis and leukocyte infiltration. Injured vascular endothelium upregulates the adhesion molecules and releases the leukocytes chemoattractant factors which eventually result in enhanced leukocyte adhesion molecules and recruitment into injured brain parenchyma. (Stahel, and Shohami et al., 2000; Lucas et al., 2006; Schoettle and Kochanek, et al., 1990).
Early BBB disruption after injury is concomitant with an acute neutrophil infiltration into injured parenchyma, peaking between 24hpi and 3dpi (Gyoneva and Ransohoff et al., 2015; Jin and Ishii et al., 2012). Neutrophils are the first leukocytes recruited into the injured parenchyma and could greatly exacerbate the tissue damage by producing and releasing numerous toxic substances namely lysosomal enzymes such myeloperoxidase, reactive oxygen species (ROS) and

reactive nitrogen species (NOS) as well as cytokines and chemokines such as TNF-α, IL-1β and IL-8, which amplify the recruitment and activation of more neutrophils to the site of injury, through the upregulation of endothelial adhesion molecules (Liu Yang-Wuyue et al., 2018). Thus, acute inflammatory mechanisms, vascular permeability and leukocyte infiltration, influence secondary post-traumatic tissue damage. Further studies indicated that neutrophils are observed only in areas exhibiting BBB damage and are initially found in injured cortex, and areas with damaged BBB within 12 h after injury, lining the vasculature and filling subarachnoid/subdural spaces. Then, neutrophils migrate from the damaged vasculature into traumatized cortical and hippocampal parenchyma by 24 h (Soares et al., 1995).

Our results described that vascular breakdown was observed in both WT and GFAP-IL10Tg animals at 24h and 3dpi. Remarkably, astrocyte-targeted production of IL-10 strongly attenuates the permeable abnormalities of the BBB at 24hpi accompanied by a significant decrease in neutrophil recruitment into the injured parenchyma. These findings support previous studies that assessed the effect of IL-10 on BBB disruption and leukocyte infiltration after acute brain injury demonstrating a similar effect (Chen and Duan et al., 2014; Kline et al., 2002). Taking into an account that neutrophils are one of the peripheral inflammatory cells entering the parenchyma of the injured brain at the early hours (24hpi-3dpi) after TBI, together with the fact that a reduction in neutrophil infiltration has been associated with a reduction in lesion size and neurological deficit in experimental transient ischaemic injuries (Connolly et al.,1996, Chen et al., 1994), lead us to speculate that IL-10 in our work is modifying the vasculature inhibiting the infiltration of inflammatory neutrophils and decreasing then the neurodegeneration.

5. Transgene production of IL-10 increased T-cell recruitment after TBI.

In addition to modifications in microglia/macrophages activation, neutrophils and monocytes infiltration as well as BBB leakage, and consistent with other reports (Jin and Ishii et al., 2012; Holmin and Soderlund et al., 1998, Dressler et al., 2007), we observed accumulation of infiltrated $CD3^+$ T cells at the penumbra of perilesional brain parenchyma after TBI. Interestingly, the proportion of $CD3^+$ T cells in GFAP-IL10Tg animals was significantly higher, suggesting a role of IL-10 on the mechanism underlying T-cell recruitment. Similar results were reported using the same transgenic animal after facial nerve axotomy and perforant pathway transection (Villacampa et al., 2015, Recasens et al., 2018). This increased infiltration of T-cells in transgenic mice cannot be explained by modifications in the BBB itself, because in contrast, as already discussed in the previous section, BBB leakage in transgenic animals was lower than in WT. Then, the better explanation could be that the increase in T-cell infiltration is related to alterations in the chemokines responsible of T-cell recruitment. Indeed, changes in these chemokines are the responsible of the higher infiltration observed after perforant

pathway transection (Recasens et al., 2019). However, we did not detect any significant modification in MCP1, the principal chemoattractant protein analyzed in our study, suggesting it will be necessary to analyse the effect of IL-10 on other molecules related to T-cell infiltration such as integrins and endothelial cell adhesion molecules (Lopes Pinheiro et al 2016).

The specific role of lymphocyte infiltration after TBI was poorly understood. It is known that T cells infiltrated the brain parenchyma in TBI during acute and chronic phases (Jin and Ishii et al., 2012; Ndode-Ekane et al., 2018) and some studies demonstrated that T cells exacerbated the posttraumatic tissue damage between 3-5 days post-injury. (Jin and Ishii et al., 2012; Timaru-Kast et al., 2012). However, Weckbach (2012) reported that Rag1 $^{-/-}$ mice, lacking T cells, are not different from wild-type mice in terms of injury severity and neurologic impairment after a closed head injury (Weckbach et al., 2012). According to our results, linking more neuroprotection with higher recruitment of T-cells, we could speculate that the role of these lymphocytes was protective. However, in our hands we cannot discard the possibility that differences in the amount of T-cells could be the consequence of the lower neurodegeneration and the modifications in neutrophil infiltration, rather than the direct cause of this protection

6. Astrocyte-targeted production of IL-10 reduces the astrocyte response, the principal cell type expressing the IL-10R1.

Activation of astrocytes under TBI has been long described in different experimental models (Villapol et al., 2014; Myer et al., 2006; Di Giovanni and Movsesyan et al., 2005). Once activated these glial cells produce a wide-range of molecules associated with the neuroinflammatory response including cytokines and growth factors (Zamanian et al., 2012).

In this work we demonstrated a decrease in the levels of GFAP on astrocytes of transgenic animals at 3dpi, coinciding with the time where higher number of infiltrated monocytes and T-cells were also observed. These effects, together with our results showing less degenerative neurons at 3dpi, makes us to suggest that IL-10 is producing a decrease in the neuroinflammatory environment of the lesioned area contributing to the lower neurodegeneration observed. In this sense, we found a significant decrease of IL-1β expression levels at 24hpi in GFAP-IL10Tg mice.

In fact, astrocytes play a key role in the maintenance of CNS physiological homeostasis (Chen and Swanson et al., 2003) and BBB integrity (Abbott and Ronnback et al., 2006). It is also generally accepted that under pathological conditions astrocytes are key in the control of peripheral immune cells, by secreting various cytokines and promoting BBB disruption, (Liu and Chopp et al 2015; Pineau et al., 2010). Thus, alterations in astrocyte could be underlying the differences observed in the BBB in our study, reinforcing our hypothesis that the effect of IL-10 is to reduce the neuroinflammatory response associated to TBI avoiding the spread of the secondary injury.

Furthermore, an in agreement with other studies (Almolda et al., 2015; Gonzalez et al., 2009; Ledeboer et al.,2002; Norden et al., 2014), we observed the expression of IL-10R1 abundantly on astrocytes at all time points of the study, being the first description following traumatic brain injury. This indicates that the effect that we have found on both neurons and microglia are probably not a direct effect of the cytokine over these cell populations but instead is an indirect effect mediated by the IL-10 function on astrocytes.

Dynamic interaction between microglia and astrocytes mediating by cytokines have been described in some studies (Abutbul et al., 2012; Schilling et al., 2001; Norden et al ., 2104). Outcomes from as study by Norden and his colleges showed that astrocyte response to IL-10 stimulation by secretion of TGF-β and TGF-β signalling down regulates LPS-activated microglial activation associated by reduction in pro-inflammatory cytokines such as IL-1β, IL-6, CCL2, TNFα (Norden et al., 2014). Further studies are mandatory to analyse the principal astrocyte-microglia communication molecules in order to decipher the specific role exerted by IL-10 after TBI.

Conclusions

After TBI, astrocyte-targeted production of IL-10:

1. Attenuates neuronal degeneration after at early time points.
2. Downregulates the microglia/macrophage activation but induces a higher phagocytic capacity to these cells.
3. Reduces the astrocytic reactivity.
4. Enhances the infiltration of inflammatory monocytes into the CNS, contributing to the higher number of microglia/macrophages observed in these animals.
5. Reduces neutrophil infiltration into injured brain at early time-points.
6. Induced an increase of T lymphocytes recruitment into the injured brain.
7. Decrease BBB permeability at 24h after injury.
8. Modified the cytokine/chemokine microenvironment, reducing the expression of the pro-inflammatory IL-1β.
9. The principal cells expressing the IL-10R1 are degenerating neurons and reactive astrocytes near the lesion core.

Altogether we conclude that astrocyte-targeted production of IL-10, through the effects on neurons and astrocytes, is modifying the neuroinflammatory response associated to TBI, increasing the phagocytic activity of microglia, reducing the BBB permeability and neutrophil infiltration and increasing the T-cell infiltration. These modifications reduce the secondary injury and lead to a better outcome of the lesion by attenuating the neurodegeneration (Figure 21).

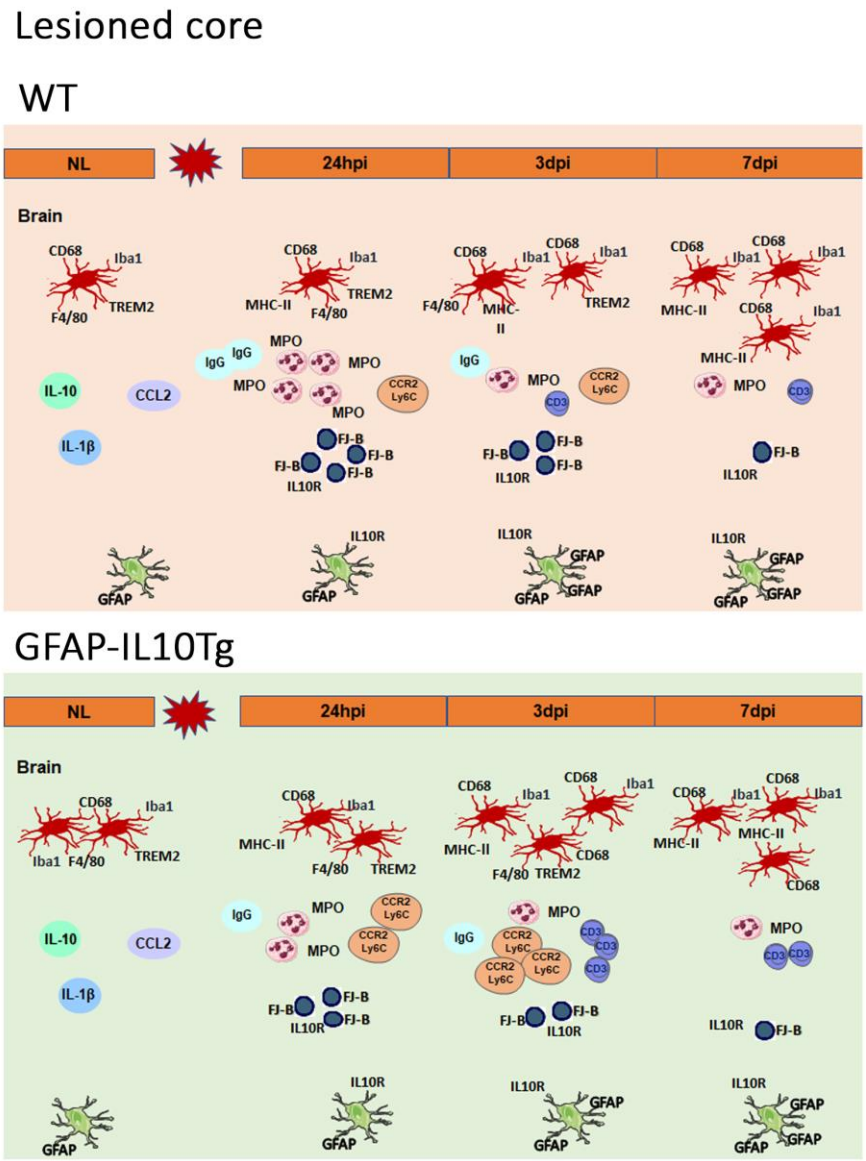

Figure 21. Inflammatory response after TBI. The principal results obtained in this work are represented in the Figure.

Bibliography

Coronado V. G., L. Xu, Basavaraju SV, McGuire LC, Wald MM, Faul MD, Guzman BR, Hemphill De. 2011. Surveillance for traumatic brain injury-related deaths--United States, 1997-2007. MMWR Surveill Summ 60:1-32.

Greve MW, Zink BJ. 2009. Pathophysiology of traumatic brain injury. Mt Sinai J Med. 76:97–104.

Ghajar J. 2000. Traumatic brain injury. Lancet 356:923-929.

Thornhill S, Teasdale GM, Murray GD, McEwen J, Roy CW, Penny KI. 2000. Disability in young people and adults one year after head injury: prospective cohort study. BMJ 320:1631-1635.

Masel B.E, DS DeWitt. 2010. Traumatic brain injury: a disease process, not an event. J.Neurotrauma 27:1529-1540.

Cederberg D, Siesjo P. 2010. What has inflammation to do with traumatic brain injury? Childs Nerv Syst 26:221–226.

Cole PJ.1986. Inflammation: a two-edged sword--the model of bronchiectasis. Eur J Respir Dis Suppl 147:6-15.

Hagemann T, Balkwill F, Lawrence T. 2007. Inflammation and cancer: a double-edged sword. Cancer Cell 12:300-301.

Doyle KP, Buckwalter MS. 2012.The double-edged sword of inflammation after stroke: what sharpens each edge? Ann Neurol 71:729-731.

Cerecedo-Lopez CD, Kim-Lee JH, Hernandez D, Acosta S, Borlongan CV. 2014. Insulin-associated neuroinflammatory pathways as therapeutic targets for traumatic brain injury. Med Hypotheses 82:171-174.

Klatzo I, Piraux A, Laskowski EJ.1958. The relationship between edema, blood brain-barrier and tissue elements in a local brain injury. J Neuropathol Exp Neurol 17:548-564.

Albert-Weissenberger C, Sirén AL. 2010. Experimental traumatic brain injury. Exp Transl Stroke Med 13:1-6.

Raslan F, Schwarz T, Meuth SG, Austinat M, Bader M, Renne T, Roosen K, Stoll G, Sirén AL, Kleinschnitz C. 2010. Inhibition of bradykinin receptor B1 protects mice from focal brain injury by reducing blood-brain barrier leakage and inflammation. J Cereb Blood Flow Metab 30:1477-1486.

Sire´n AL, Radyushkin K, Boretius S, Kammer D, Riechers CC, Natt O, Sargin D, Watanabe T, Sperling S, Michaelis T, Price J, Meyer B, Frahm J, Ehrenreich H. 2006. Global brain atrophy after unilateral parietal lesion and its prevention by erythropoietin. Brain 129:480–489.

Kabadi SV, Hilton GD, Stoica BA, Zapple DN, Faden AI. 2010. Fluid-percussion-induced traumatic brain injury model in rats. Nature Protoc 5:1552–1563.

Dixon CE, Clifton GL, Lighthall JW, Yaghmai AA, Hayes RL. 1991. A controlled cortical impact model of traumatic brain injury in the rat. J Neurosci Methods 39:253–262.

Lighthall JW, Goshgarian HG, Pinderski CR.1990.Characterization of axonal injury produced by controlled cortical impact. J Neurotrauma 7:65–76.

Morales DM, Marklund N, Lebold D, Thompson HJ, Pitkanen A, Maxwell WL, Longhi L, Laurer H, Maegele M, Neugebauer E, Graham DI, Stocchetti N, McIntosh TK. 2005. Experimental models of traumatic brain injury: do we really need to build a better mousetrap? Neuroscience 136:971–989.

Albert-Weissenberger C, Varrallyay C, Raslan F, Kleinschnitz C, Siren AL. 2012. An experimental protocol for mimicking pathomechanisms of traumatic brain injury in mice. Exp Transl Stroke Med 4:1-5.

Feeney DM, Boyeson MG, Linn RT, Murray HM, Dail WG. Responses to cortical injury: I. Methodology and local effects of contusions in the rat.1981. Brain Res 211:67–77.

Soares HD, Hicks RR, Smith D, McIntosh TK.1995. Inflammatory leukocytic recruitment and diffuse neuronal degeneration are separate pathological processes resulting from traumatic brain injury. J Neurosci 15:8223–8233.

Ziebell JM, Morganti-Kossmann MC. 2010. Involvement of pro- and anti-inflammatory cytokines and chemokines in the pathophysiology of traumatic brain injury. Neurotherapeutics 7:22-30.

Manson J, Thiemermann C, Brohi K. 2012. Trauma alarmins as activators of damage-induced inflammation. Br J Surg 1:12–20.

Gurley C, Nichols J, Liu S, Phulwani NK, Esen N, Kielian T. 2008. Microglia and astrocyte activation by toll-like receptor ligands: modulation by PPARgamma agonists. PPAR Res 453120.

Kigerl KA, de Rivero Vaccari JP, Dietrich WD, Popovich PG, Keane RW. 2014. Pattern recognition receptors and central nervous system repair. Exp Neurol 258:5–16.

Nagyoszi P, Wilhelm I, Farkas AE, Fazakas C, Dung NT, Hasko J, Krizbai IA. 2010. Expression and regulation of toll-like receptors in cerebral endothelial cells. Neurochem Int 57:556–564.

Dalgard CL, Cole JT, Kean WS, Lucky JJ, Sukumar G, McMullen DC, Pollard HB,Watson WD. 2012. The cytokine temporal profile in rat cortex after controlled cortical impact. Front Mol Neurosci 5:1-6.

Rhodes J. 2011. Peripheral immune cells in the pathology of traumatic brain injury? Curr Opin Crit Care 17:122–130.

Hsieh CL, Kim CC, Ryba BE, Niemi EC, Bando JK, Locksley RM, Liu J, Nakamura MC, Seaman WE. 2013. Traumatic brain injury induces macrophage subsets in the brain. Eur J Immunol 43:2010–2022.

Liu Yang-Wuyue, Li Song, Dai Shuang-Shuang.2018. Neutrophils in traumatic brain injury (TBI): friend or foe? J Neuroinflammation 15:146.

Holmin S, Mathiesen T, Shetye J, Biberfeld P.1995. Intracerebral inflammatory response to experimental brain contusion. Acta Neurochir 132:110–119.

Kelley BJ, Lifshitz J, Povlishock JT. 2007. Neuroinflammatory responses after experimental diffuse traumatic brain injury. J Neuropathol Exp Neurol 66:989–1001.

Gyoneva S, Ransohoff RM. 2015. Inflammatory reaction after traumatic brain injury: therapeutic potential of targeting of cell-cell communication by chemokines. Trends Pharmacol Sci 36:471-80.

Ransohoff RM. 2016. A polarizing question: do M1 and M2 microglia exist? Nat. Neurosci 19:987–991.

Gordon S. 2003. Alternative activation of macrophages. Nat Rev Immunol 3:23–35.

Sica A, Mantovani A. 2012.Macrophage plasticity and polarization: in vivo veritas. J Clin Invest 122:787–795.

Colton CA. 2009. Heterogeneity of microglial activation in the innate immune response in the brain. J Neuroimmune Pharmacol 4:399–418.

Filardy AA, Pires DR, Nunes MP, Takiya CM, Freire-de-Lima CG, Ribeiro-Gomes FL, DosReis GA. 2010. Proinflammatory clearance of apoptotic neutrophils induces an IL-12(low) IL-10(high) regulatory phenotype in macrophages. J Immunol 185:2044–2050.

Kumar A, Alvarez-Croda DM, Stoica BA, Faden AI, Loane DJ. 2016. Microglial/Macrophage Polarization Dynamics following Traumatic Brain Injury. J Neurotrauma 33:1732-1750.

Kigerl KA, Gensel JC, Ankeny DP, Alexander JK, Donnelly DJ, Popovich PG. 2009. Identification of two distinct macrophage subsets with divergent effects causing either neurotoxicity or regeneration in the injured mouse spinal cord. J Neurosci 29:13435–13444.

Wang G, Zhang J, Hu X, Zhang, L, Mao L, Jiang X, Liou AK, Leak RK, Gao Y, Chen J. 2013. Microglia/macrophage polarization dynamics in white matter after traumatic brain injury. J Cereb Blood Flow Metab 33:1864–1874.

Loane DJ, Kumar A. 2016. Microglia in the TBI brain: The good, the bad, and the dysregulated. Exp Neurol 3:316-327.

Zamanian JL, Xu L, Foo LC, Nouri N, Zhou L, Giffard RG et al. 2012. Genomic analysis of reactive astrogliosis J Neurosci 32:6391–6410.

Paintlia MK, Paintlia AS, Singh AK, Singh I. 2013. S-nitrosoglutathione induces ciliary neurotrophic factor expression in astrocytes that has implication to protect CNS under pathological conditions. J Biol Chem 288:3831–3843.

Villapol S, Byrnes KR, Symes AJ. 2014. Temporal dynamics of cerebral blood flow, cortical damage. Apoptosis 5:82.

Myer DJ, Gurkoff GG, Lee SM, Hovda DA, Sofroniew MV. 2006. Essential protective roles of reactive astrocytes in traumatic brain injury. Brain 129: 2761–2772.

Di Giovanni S, Movsesyan V, Ahmed F, Cernak I, Schinelli S, Stoica B et. 2005. Cell cycle inhibition provides neuroprotection and reduces glial proliferation and scar formation after traumatic brain injury. Proc Natl Acad SciUSA 102: 8333–8338.

Silver J, Miller JH. 2004. Regeneration beyond the glial scar. Nat Rev Neurosci 5:146–156.

Ribotta MG, Menet V, Privat A. 2004. Glial scar and axonal regeneration in the CNS: lessons from GFAP and vimentin transgenic mice. Acta Neurochir Suppl 89:87–92.

Jin X, Ishii H, Bai Z, Itokazu T, Yamashita T. 2012. Temporal changes in cell marker expression and cellular infiltration in a controlled cortical impact model in adult male C57BL/6 mice. PLoS One 7:e41892.

Kenne E, Erlandsson A, Lindbom L, Hillered L, Clausen F. 2012. Neutrophil depletion reduces edema formation and tissue loss following traumatic brain injury in mice. J Neuroinflammation 9:17.

Knoblach SM, Faden AI. 2002. Administration of either anti intercellular adhesion molecule-1 or a nonspecific control antibody improves recovery after traumatic brain injury in the rat. J Neurotrauma 19:1039–1050.

Carlos TM, Clark RS, Franicola-Higgins D, Schiding GK, Kochaneck PMP. 1997. Expression of endothelial adhesion molecules and recruitment of neutrophils after traumatic brain injury in rats. J Leukoc Biol 61:279–285.

Weaver KD, Branch CA, Hernandez L, Miller CH, Quattrocchi KB. 2000. Effect of leukocyte-endothelial adhesion antagonism on neutrophil migration and neurologic outcome after cortical trauma. J Trauma 48:1081–1090.

Semple BD, Bye N, Ziebell JM, Morganti-Kossmann MC. 2010.Deficiency of the chemokine receptor CXCR2 attenuates neutrophil Infiltration and cortical damage following closed head injury. Neurobiol.Dis 40:394–403.

Mildner A, Marinkovic G, Jung S 2016. Monocytes: Origins, Subsets, Fates, and Functions. Microbiolspec 4:5-15.

Semple D, Bye N, Rancan M, Jenna M, Morganti-Kossmann MC 2009. Role of CCL2 (MCP-1) in Traumatic Brain Injury (TBI): Evidence from Severe TBI Patients and CCL2−/− Mice. J Cereb Blood Flow Metab 30:769-782.

Ginhoux F, Greter M, Leboeuf M, Nandi S, See P, Gokhan S, Mehler MF, Conway SJ, Ng LG, Stanley ER, Samokhvalov IM, Merad M. 2010. Fate mapping analysis reveals that adult microglia derive from primitive macrophages. Science 330:841–845.

Butovsky O, Jedrychowski MP, Moore CS, Cialic R, Lanser AJ, Gabriely G, Koeglsperger T, Dake B, Wu PM, Doykan CE, Fanek Z, Liu L, Chen Z, Rothstein JD, Ransohoff RM, Gygi SP, Antel JP, Weiner HL. 2014. Identification of a unique TGF-β–dependent molecular and functional signature in microglia. Nat Neurosci 17:131–143.

Yamasaki R, Lu H, Butovsky O, Ohno N, Rietsch AM, Cialic R, Ransohoff RM. 2014. Differential roles of microglia and monocytes in the inflamed central nervous system. J Exp Med 211:1533-1549.

Reiner SL. 2009. Decision making during the conception and career of CD4+ T cells. Nat Rev Immunol 9:81–82.

Zhu J, Yamane H, Paul WE. 2010. Differentiation of effector CD4 T cell populations. Annu Rev Immunol 28:445–89.

Zhang N, Bevan MJ. 2011. CD8(+) T cells: foot soldiers of the immune system. Immunity. 35:161–168.

Holmin S, Soderlund J, Biberfeld P, Mathiesen T.1998. Intracerebral inflammation after human brain contusion. Neurosurgery 42:291–298.

Dressler J, Hanisch U, Kuhlisch E, Geiger KD. 2007. Neuronal and glial apoptosis in human traumatic brain injury. Int J Legal Med 121:365–375.

Clausen F, Lorant T, Lewen A, Hillered L. 2007. T lymphocyte trafficking: a novel target for neuroprotection in traumatic brain injury. J Neurotrauma 24:1295–307.

Fee D, Crumbaugh A, Jacques T, Herdrich B, Sewell D, Auerbach D, Piaskowski S, Hart MN, Sandor M, Fabry Z. 2003. Activated/effector CD4+ T cells exacerbate acute damage in the central nervous system following traumatic injury. J Neuroimmunol 136:54–66.

Krämer TJ, Hack N, Brühl TJ, Menzel L, Hummel R, Griemert EV, Klein M, Thal SC, Bopp T, Schäfer MKE. 2019. Depletion of regulatory T cells increases Tcell brain infiltration, reactive astrogliosis, and interferon-γ gene expression in acute experimental traumatic brain injury. J Neuroinflammation 16:163-176.

Yang C, Hawkins KE, Doré S, Candelario-Jalil E. 2019. Neuroinflammatory mechanisms of blood-brain barrier damage in ischemic stroke. Am J Physiol Cell Physiol 316:135-153.

Zlokovic BV. 2011. Neurovascular pathways to neurodegeneration in Alzheimer's disease and other disorders. Nat Rev Neurosci 12:723-738.

Kirk J, Plumb J, Mirakhur M, Mcquaid S. 2003. Tight junctional abnormality in multiple sclerosis white matter affects all calibres of vessel and is associated with blood-brain barrier leakage and active demyelination. J Pathol 201:319- 327.

Habgood MD, Bye N, Dziegielewska KM, Ek CJ, Lane MA, Potter A, Morganti-Kossman CM, Saunders NR. 2007. Changes in blood-brain barrier permeability to large and small molecules following traumatic brain injury in mice. Eur J Neurosci 25:231–238.

Povlishock JT, Becker DP, Sullivan HG, Miller JD. 1978. Vascular permeability alterations to horseradish peroxidase in experimental brain injury. Brain Res. 22:223– 239.

Dietrich WD, Alonso O, Halley M. 1994. Early microvascular and neuronal consequences of traumatic brain injury: a light and electron microscopic study in rats. J Neurotrauma 11:289–301.

Stahel PF, Shohami E, Younis FM, Kariya K, Otto VI, Lenzlinger PM, Grosjean MB, Eugster HP, Trentz O, Kossmann T, Morganti-Kossmann MC. 2000. Experimental

closed head injury: analysis of neurological outcome, blood-brain barrier dysfunction, intra-cranial neutrophil infiltration, and neuronal cell death in mice deficient in genes for pro-inflammatory cytokines. J Cereb Blood Flow Metab 20:369–380.

Lucas SM, Rothwell NJ, Gibson RM. 2006. The role of inflammation in CNS injury and disease. Brit J Pharmacol 147:232–240.

Stahel PF, Morganti-Kossmann MC, Perez D, Redaelli C, Gloor B, Trentz O, Kossmann T. 2001. Intrathecal levels of complement-derived soluble membrane attack complex (sC5b-9) correlate with blood-brain barrier dysfunction in patients with traumatic brain injury. J Neurotrauma 18:773-781.

Saw MM, Chamberlain J, Barr M, Morgan MP, Burnett JR, Ho KM. 2014. Differential disruption of blood-brain barrier in severe traumatic brain injury. Neurocrit Care 20:209-216

Schoettle RJ, Kochanek PM, Magargee MJ, Uhl MW, Nemoto EM. 1990. Early polymorphonuclear leukocyte accumulation correlates with the development of posttraumatic cerebral edema in rats. J.Neurotrauma 7:207–217.

Lu J, Moochhala S, Kaur C, Ling EA. 2001. Cellular inflammatory response associated with breakdown of the blood-brain barrier after closed head injury in rats. J Neurotrauma 18:399–408.

Block ML, Zecca L, Hong JS. 2007. Microglia-mediated neurotoxicity: uncovering the molecular mechanisms.Neuroscience 8:57-69.

Mukherjee S, Katki K, Arisi GM, Foresti ML, Shapiro LA. 2011. Early TBI-induced cytokine alterations are similarly detected by two distinct methods of multiplex assay. Front Mol Neurosci 4:21.

Harting MT, Jimenez F, Adams SD, Mercer DW, Cox CS. 2008. Acute, regional inflammatory response after traumatic brain injury: implications for cellular therapy. Surgery 144:803–813.

Shohami E, Gallily R, Mechoulam R, Bass R, Ben-Hur T. 1997. Cytokine production in the brain following closed head injury: dexanabinol (HU-211) is a novel TNF-inhibitor and an effective neuroprotectant. J Neuroimmunol 72:169 –177.

Allan SM, Rothwell NJ. 2001. Cytokines and acute neurodegeneration. Nat Rev Neurosci 2:734 –744.

Chao CC, Hu S, Ehrlich L, Peterson PK. 1995. Interleukin-1 and tumor necrosis factor- synergistically mediate neurotoxicity: involvement of nitric oxide and of N-methyl-D-aspartate receptors. Brain Behav Immun 9:355–365.

Rankine EL, Hughes PM, Botham MS, Perry VH, Felton LM. 2006. Brain cytokine synthesis induced by an intraparenchymal injection of LPS is reduced in MCP-1-deficient mice prior to leucocyte recruitment. Eur J Neurosci 24:77– 86.

Couper KN, Blount DG, Riley EM, 2008. IL-10: the master regulator of immunity to infection. J Immunol 180:5771–5777.

Moore KW, de Waal Malefyt R, Coffman RL, O'Garra A. 2001. Interleukin-10 and the interleukin-10 receptor. Annu Rev Immunol 19:683–765.

Kamm K, Vanderkolk W, Lawrence C, Jonker M, Davis AT. 2006. The effect of traumatic brain injury upon the concentration and expression of interleukin-1beta and interleukin-10 in the rat. J Trauma 60:152–157.

Zhai QH, Futrell N, Chen FJ. 1997. Gene expression of IL-10 in relationship to TNF-alpha, IL-1beta and IL-2 in the rat brain following middle cerebral artery occlusion. J Neurol Sci 152:119–124.

Gonzalez P, Burgaya F, Acarin L, Peluffo H, Castellano B, Gonzalez B. 2009. Interleukin-10 and interleukin-10 receptor-I are upregulated in glial cells after an excitotoxic injury to the postnatal rat brain. J Neuropathol Exp Neurol 68:391–403.

Apelt J, Schliebs R. 2001. Beta-amyloid-induced glial expression of both pro- and anti-inflammatory cytokines in cerebral cortex of aged transgenic Tg2576 mice with Alzheimer plaque pathology. Brain Res 894:21–30.

Hulshof S, Montagne L, De Groot CJ, Van Der Valk P. 2002. Cellular localization and expression patterns of interleukin-10, interleukin-4, and their receptors in multiple sclerosis lesions. Glia 38:24–35

Ledeboer A, Wierinckx A, Bol JG, Floris S, Renardel de Lavalette C, De Vries HE, van den Berg TK, Dijkstra CD, Tilders FJ, van dam AM. 2003. Regional and temporal expression patterns of interleukin-10, interleukin-10 receptor and adhesion molecules in the rat spinal cord during chronic relapsing EAE. J Neuroimmunol 136:94–103.

Csuka E, Morganti-Kossman MC, Lenzlinger PM, Joller H, Trentz O, Kossmann T. 1999. IL-10 levels in cerebrospinal fluid and serum of patients with severe traumatic brain injury: relationship to IL-6, TNF-, TGF-1 and blood-brain barrier function. J Neuroimmunol 101:211–221.

Ledeboer A, Breve JJ, Wierinckx A, van der Jagt S, Bristow AF, Leysen JE, Tilders FJ, Van Dam AM. 2002. Expression and regulation of interleukin-10 and interleukin-10 receptor in rat astroglial and microglial cells. Eur J Neurosci 16:1175–1185.

Norden DM, Fenn AM, Dugan A, Godbout JP. 2014. TGFbeta produced by IL-10 redirected astrocytes attenuates microglial activation. Glia 62:881–895.

Cannella, B., Raine, C.S., 2004. Multiple sclerosis: cytokine receptors on oligodendrocytes predict innate regulation. Ann. Neurol. 55, 46–57.

Lodge PA, Sriram S.1996. Regulation of microglial activation by TGF-beta, IL-10, and CSF-1. J Leukoc Biol 60:502–508.

Balasingam V, Yong V.1996. Attenuation of astroglialreactivity by interleukin-10. J Neurosci16: 2945–2955.

Bethea JR, Nagashima H, Acosta MC, Briceno C, Gomez F, Marcillo AE, Loor K, Green J, Dietrich WD. 1999. Systemically administered interleukin-10 reduces tumor necrosis factor-alpha production and significantly improves functional recovery following traumatic spinal cord injury in rats. J Neurotrauma 16:851–863.

Ooboshi H, Ibayashi S, Shichita T, Kumai Y, Takada J, Ago T, Arakawa S, Sugimori H, Kamouchi M, Kitazono T, Iida M. 2005. Postischemic gene transfer of interleukin-10 protects against both focal and global brain ischemia. Circulation 111:913 919.

Arimoto T, Choi DY, Lu X, Liu M, Nguyen XV, Zheng N, Stewart CA, Kim HC, Bing G. 2007. Interleukin-10 protects against inflammation-mediated degeneration of dopaminergic neurons in substantia nigra. Neurobiol Aging 28:894–906.

Bachis A, Colangelo AM, Vicini S, Doe PP, De Bernardi MA, Brooker G, Mocchetti I. 2001. Interleukin-10 prevents glutamate-mediated cerebellar granule cell death by blocking caspase-3-like activity. J Neurosci 21:3104–3112.

Brewer KL, Bethea JR, Yezierski RP. 1999. Neuroprotective effects of interleukin-10 following excitotoxic spinal cord injury. Exp Neurol 159:484– 493.

Knoblach SM, Faden AI. 1998. Interleukin-10 improves outcome and alters proinflammatory cytokine expression after experimental traumatic brain injury. Exp Neurol 153:143–51.

Ledeboer A, Breve JJ, Poole S, Tilders FJ, Van Dam AM. 2000. Interleukin-10, interleukin-4, and transforming growth factor-beta differentially regulate lipopolysaccharide-induced production of pro-inflammatory cytokines and nitric oxide in co-cultures of rat astroglial and microglial cells. Glia 30:134–142.

Molina-Holgado E, Vela JM, Arevalo-Martin A, Guaza C. 2001. LPS/IFN-gamma cytotoxicity in oligodendroglial cells: role of nitric oxide and protection by the anti-inflammatory cytokine IL-10. Eur J Neurosci 13:493–502.

Park KW, Lee HG, Jin BK, Lee YB. 2007. Interleukin-10 endogenously expressed in microglia prevents lipopolysaccharide-induced neurodegeneration in the rat cerebral cortex in vivo. Exp Mol Med 39:812– 819.

Spera PA, Ellison JA, Feuerstein GZ, Barone FC. 1998. IL-10 reduces rat brain injury following focal stroke. Neurosci Lett 251:189–192.

Xin J, Wainwright DA, Mesnard NA., Serpe CJ, Sanders VM, Jones KJ. 2011. IL-10 within the CNS is necessary for CD4+ Tcells to mediate neuroprotection. Brain Behav Immun 25:820–829.

Almolda B, de Labra C, Barrera I, Gruart A, Delgado-Garcia JM, Villacampa N, Castellano B. 2015. Alterations in microglial phenotype and hippocampal neuronal function in transgenic mice with astrocyte-targeted production of interleukin-10. Brain Behav Immun 45:80–97.

Almolda B, Costa M, Montoya M, Gonzalez B & Castellano B. 2009. CD4 microglial expression correlates with spontaneous clinical improvement in the acute Lewis rat EAE model. Journal of Neuroimmunology, 209(1–2), 65–80.

Sato M, Chang E, Igarashi T, Noble LJ. 2001. Neuronal injury and loss after traumatic brain injury: time course and regional variability. Brain Res 917:45-54.

Clark RS, Kochanek PM, Dixon CE, Chen M, Marion DW, Heineman S, DeKosky ST, Graham SH. 1997. Early neuropathologic effects of mild or moderate hypoxemia after controlled cortical impact injury in rats. J Neurotrauma 14:179–189.

Conti AC1, Raghupathi R, Trojanowski JQ, McIntosh TK.1998. Experimental brain injury induces regionally distinct apoptosis during the acute and delayed post-traumatic period. J Neurosci 18:5663–5672.

Fox GB, Fan L, Levasseur RA, Faden AI.1998. Sustained sensory / motor and cognitive deficits with neuronal apoptosis following controlled cortical impact brain injury in the mouse. J Neurotrauma 15:599–614.

Villacampa N, Almolda B, Vilella A, Campbell IL, Gonzalez B, Castellano B. 2015. Astrocyte-targeted production of IL-10 induces changes in microglial reactivity and reduces motor neuron death after facial nerve axotomy. Glia 63:1166–1184.

Recasens M, Shrivastava K, Almolda B, González B, Castellano B. 2018. Astrocyte-targeted IL-10 production decreases proliferation and induces a downregulation of activated microglia/macrophages after PPT. Glia 67:741–758.

Susarla BT, Villapol S, Yi JH, Geller HM, Symes AJ. 2014. Temporal patterns of cortical proliferation of glial cell populations after traumatic brain injury in mice. ASN Neuro 6:159–170. Strle K, Zhou JH, Broussard SR, Venters HD, Johnson RW, Freund GG, Kelley KW. 2002. IL-10 promotes survival of microglia without activating Akt. J Neuroimmun 122:9–19.

Strle K, Zhou JH, Broussard SR, Venters HD, Johnson RW, Freund GG, Dantzer R, Kelley KW. 2002. IL-10 promotes survival of microglia without activating Akt. J Neuroimmunol 122:9–19.

Sawada M, Suzumura A, Hosoya H, Marunouchi T, Nagatsu T.1999. Interleukin-10 inhibits both production of cytokines and expression of cytokine receptors in microglia. J Neurochem 72:1466–1471.

Loane DJ, Kumar A, Stoica BA, Cabatbat R, Faden AI. 2014. Progressive neurodegeneration after experimental brain trauma: association with chronic microglial activation. J Neuropathol Exp Neurol 73:14–29.

Mizuno T, Sawada M, Marunouchi T, Suzumura A.1994. Production of interleukin-10 by mouse glial cells in culture. Biochem Biophys Res Commun 205:1907–1915.

De Waal Malefyt R, Haanen J, Spits H, Roncarolo MG, Te Velde A, Figdor C, Johnson K, Kastelein R, Yssel H, De Vries JE. 1991. Interleukin 10 (IL-10) and viral IL-10 strongly reduce antigen-specific human T cell proliferation by diminishing the antigen-presenting capacity of monocytes via downregulation of class II major histocompatibility complex expression. J Exp Med 174:915–924.

Enk AH, Angeloni VL, Udey MC, Katz SI. 1993. Inhibition of Langerhans cell antigen-presenting function by IL-10, a role for IL-10 in induction of tolerance. J Immunol 151:2390–2398.

Fluckiger AC, Garrone P, Durand I, Galizzi JP, Banchereau J. 1993. Interleukin 10 (IL-10) upregulates functional high affinity IL-2 receptors on normal and leukemic B lymphocytes. J Exp Med. 178:1473–1481.

Lotocki G, de Rivero Vaccari JP, Perez ER, Sanchez-Molano J, Furones-Alonso O, Bramlett HM, Dietrich WD. 2009. Alterations in Blood-Brain Barrier Permeability to Large and Small Molecules and Leukocyte Accumulation after Traumatic Brain Injury: Effects of Post-Traumatic Hypothermia. J Neurotrauma 26:1123–1134.

Chen X, Duan XS, Xu LJ, Zhao JJ, She ZF, Chen WW, Zheng ZJ, Jiang GD. 2014. Interleukin-10 mediates the neuroprotection of hyperbaric oxygen therapy against traumatic brain injury in mice. Neuroscience 266:235–243.

Kline AE, Bolinger BD, Kochanek PM, Carlos TM, Yan HQ, Jenkins LW, Marion DW, Dixon CE. 2002. Acute systemic administration of interleukin-10 suppresses the beneficial effects of moderate hypothermia following traumatic brain injury in rats. Brain Res 937:22–31.

Connolly ES Jr, Winfree CJ, Springer TA. 1996. Cerebral protection in homozygous null ICAM-1 mice after middle cerebral artery occlusion. Role of neutrophil adhesion in the pathogenesis of stroke. J Clin Invest 97:209–216.

Chen HM, Zhang P, Voso MT, Hohaus S, Gonzalez DA, Glass CK, Zhang DE, Tenen DG. 1995. Neutrophils and monocytes express high levels of PU.1 (Spi-1) but not Spi-B. Blood 85:2918-2928.

Lopes Pinheiro MA, Kroon J, Hoogenboezem M, Geerts D. 2016. Acid Sphingomyelinase–Derived Ceramide Regulates ICAM-1 Function during T Cell Transmigration across Brain Endothelial Cells. The Journal of Immunology196 (1) 72-79.

Ndode-Ekane XE, Matthiesen L, Banuelos-Cabrera I, CAP P, Pitkanen A. 2018. T-cell infiltration into the perilesional cortex is long-lasting and associates with poor somatomotor recovery after experimental traumatic brain injury. Restor Neurol Neurosci 36(4):485–501.

Timaru-Kast R, Luh C, Gotthardt P, Huang C, Schäfer MK, Engelhard K. 2012. Influence of age on brain edema formation, secondary brain damage and inflammatory response after brain trauma in mice. PLoS One 7:e43829.

Weckbach S, Neher M, Losacco JT, Bolden AL, Kulik L, Flierl MA, Stahel PF. 2012. Challenging the role of adaptive immunity in neurotrauma: Rag1(-/-) mice lacking mature B and T cells do not show neuroprotection after closed head injury. J Neurotrauma 29:1233-1242.

Chen Y, Swanson RA. 2003. Astrocytes and brain injury. J Cereb Blood Flow Metab 23:137–149.

Abbott NJ, Ronnback L, Hansson E. 2006. Astrocyte-endothelial interactions at the blood-brain barrier. Nat Rev Neurosci 7:41–53.

Liu Z, Chopp M. 2015. Astrocytes, therapeutic targets for neuroprotection and neurorestoration in ischemic stroke. Prog Neurobiol 144:103-120.

Pineau I, Sun L, Bastien D, Lacroix S. 2010. Astrocytes initiate inflammation in the injured mouse spinal cord by promoting the entry of neutrophils and inflammatory monocytes in an IL-1 receptor/MyD88-dependent fashion. Brain Behav Immun 24:540–553.

Abutbul S, Shapiro J, Szaingurten-Solodkin I, Levy N, Carmy Y, Baron R, Monsonego A. 2012. TGF-beta signaling through SMAD2/3 induces the quiescent microglial phenotype within the CNS environment. Glia 60:1160–1171.

Schilling T, Nitsch R, Heinemann U, Haas D, Eder C. 2001. Astrocyte-released cytokines induce ramification and outward K+ channel expression in microglia via distinct signalling pathways. Eur J Neurosci 14:463–473.